https://doi.org/10.5194/wes-2025-198
Preprint. Discussion started: 15 October 2025

eawe european academy of wind energy
Open Access WIND ENERGY SCIENCE DISCUSSIONS

Temperature profiling at the American WAKE ExperimeNt (AWAKEN): methodology and uncertainty quantification

Stefano Letizia[1], David D. Turner[2], Aliza Abraham[1], Luc Rochette[3], and Patrick J. Moriarty[1]

[1]National Renewable Energy Laboratory, Golden, CO, USA
[2]National Oceanic and Atmospheric Administration, Global Systems Laboratory, Boulder, CO, USA
[3]LR Tech, Inc., Lévis, QC, Canada

Correspondence: Stefano Letizia (stefano.letizia@nrel.gov)

Abstract. We quantify the accuracy of the temperature profiling from ground-based spectral infrared radiance observations at AWAKEN. Results from pre-campaign tests and comparisons with in-situ ground-based and airborne sensors at AWAKEN indicate that temperature profiles agree satisfactorily with traditional instruments for wind energy applications. The bias is within a fraction of a degree and appears to be related to atmospheric stability. Root-mean-square differences from the reference instruments are always smaller than a degree and are often well described by the online uncertainty estimation product. Height-to-height and site-to-site temperature differences are in excellent agreement with in-situ observations, which justifies the use of temperature profilers to characterize static stability and spatial gradients of temperature.

1 Introduction

An accurate characterization of the atmospheric state is essential to understand the mechanisms that govern the conversion of the flow of kinetic energy carried by the wind into mechanical and, ultimately, electrical power delivered to the grid by wind power plants. In fact, although wind energy represents a widely available resource and an established technology across the U.S. and globally, it introduces new challenges to the global power system due to its intermittency and uncontrollability. This is becoming a more pressing concern as the worldwide electricity demand grows by 4% annually, driven largely by electrification, air conditioning needs, and data centers (International Energy Agency, 2025).

The volatility of wind power is inherently connected to the complex dynamics of the atmospheric boundary layer (ABL) in which wind turbines operate. The ABL state is extremely difficult to predict, and current wind resource models still have significant biases (Lee and Fields, 2021; Bodini et al., 2024). A recent blind comparison of several turbine models attributed a large portion of the uncertainty to incomplete information of the inflow conditions, especially when the ABL is stably stratified (Doubrawa et al., 2020). Complexity of the wind field is further enhanced as the thermally stratified ABL interacts with even modest terrain features (Mahrt et al., 2021; Radünz et al., 2024) or the turbines themselves (Krishnamurthy et al., 2025; Abraham et al., 2025).

Atmospheric stability not only plays a role in shaping the undisturbed wind profiles experienced by the turbines but also governs the propagation of wind turbine wakes, with large implications on the overall efficiency and lifetime of the wind plant.

https://doi.org/10.5194/wes-2025-198
Preprint. Discussion started: 15 October 2025

eawe european academy of wind energy
Open Access WIND ENERGY SCIENCE DISCUSSIONS

This influence of thermal stratification on wake morphology has been largely proved in numerical (e.g. Abkar and Porté-Agel (2015)), lab-scale (e.g., Chamorro and Porté-Agel (2010)), and field-scale studies (e.g., Zhan et al. (2019)).

The importance of atmospheric stability within the physics of wind energy prompted many experts to advocate for a more comprehensive experimental characterization of the key quantities that govern the physics of the atmosphere, with particular emphasis on those that carry information on the thermal state of the ABL, primarily temperature profiles (Veers et al., 2019; Shaw et al., 2022).

Better knowledge of the temperature profiles around operating wind power plants could also help to elucidate a long-standing question about the effects of wind turbine wakes on local climate. Early coarse simulations of global weather patterns with extremely large wind penetrations showed potential climate impacts (Keith et al., 2004; Wang and Prinn, 2010; Li et al., 2018; Miller and Keith, 2018). However, experimental work using satellite-derived surface temperatures (Zhou et al., 2012, 2013; Xia et al., 2016; Liu et al., 2023; Walsh-Thomas et al., 2012) or observations near the ground (Baidya Roy and Traiteur, 2010; Rajewski et al., 2013; Smith et al., 2013; Moravec et al., 2018; Wu and Archer, 2021) highlighted temperature differences generally less than one degree that appear to be induced by turbines. The general consensus is that turbines cause surface warming during nighttime stably stratified conditions, while daytime data draw a more uncertain picture. More recent meso- and micro-scale CFD studies proposed sound physical explanations of the thermal effects of wind turbines (Xia et al., 2019; Wu et al., 2023), especially thanks to the access to simulated vertical temperature profiles. However, observations of thermal effects of wind turbines across multiple heights to support such hypotheses are still scarce.

Finally, a more practical, nevertheless important use of temperature information for wind energy is the estimation of air density profile across the turbine rotor span, which is essential to assess the energy yield and carry out power performance tests of wind turbines (International Electrotechnical Commission, 2022).

Based on the former discussion, temperature profiling has been one of the foci of the American WAKE experimeNt (AWAKEN, (Moriarty et al., 2024)), the largest experimental field campaign for wind energy conducted in the U.S. to date. At the AWAKEN site, temperature profiles were routinely measured through an innovative remote sensing tool, which combined the observations from infrared spectrometers and historical radiosonde data to estimate vertical profiles of temperature throughout the ABL and beyond. Specifically, spectrometers called ASSIST-II (Atmospheric Sounder Spectrometer by Infrared Spectral Technology, (Michaud-Belleau et al., 2025)) by LRTech were deployed at several locations throughout the AWAKEN domain and recorded the downwelling spectral infrared radiance at the ground level. The physical retrieval algorithm TROPoe (Tropospheric Remotely Observed Profiling via optimal estimation, Turner and Blumberg (2019); Turner and Löhnert (2014); Adler et al. (2024)) was then used to estimate temperature profiles that matched the observed radiance. The combined ASSIST+TROPoe system represents a thermodynamic profiler.

The AWAKEN project hosted the first large-scale deployment of thermodynamic profilers for wind energy research and included extensive validation. The TROPoe methodology is briefly described in Section 2 while the following sections discuss the details of the validation process. In the pre-campaign phase, two identical thermodynamic profilers were installed side-by-side to assess the magnitude of instrumental noise and calibration error (Section 3.2). The temperature estimated by the thermodynamic profilers was also compared to observations from a nearby met masts to quantify the overall error across different

https://doi.org/10.5194/wes-2025-198
Preprint. Discussion started: 15 October 2025

eawe european academy of wind energy
Open Access WIND ENERGY SCIENCE DISCUSSIONS

heights, mainly in the surface layer (Section 3.3). Later on, during AWAKEN, temperature profiles from a thermodynamic profiler were validated vs. radiosonde measurements, providing a comprehensive error quantification across the entire ABL (Section 4.2). Finally, differences in temperature between sites were compared to the same quantities observed by independent and co-located surface met stations to assess the ability of temperature profiling to characterize the spatial heterogeneity of the temperature field (Section 4.3). Key takeaways are provided at the end of each section, and overall conclusions are drawn in Section 5.

2 Methods

The temperature profiling method used at AWAKEN relies on the information on temperature and humidity profiles contained in the downwelling infrared spectral radiance observed at the ground by the ASSIST. This information is then combined with ancillary measurements (e.g., the cloud base height or CBH from a ceilometer) and used by TROPoe to estimate the thermodynamic state that agrees with the observed infrared radiance and has the highest likelihood based on the current observations and constrained by past climatology. The retrieved thermodynamic state includes the vertical temperature profile, as well as humidity and cloud properties, although we will focus on the first quantity in the present study. This section will review the fundamentals of temperature profiling at AWAKEN. For a more detailed discussion, the reader is referred to Letizia et al. (2025) and the references listed therein and below.

2.1 Physics of radiation in the atmosphere

The spectral radiance observed at the ground, B, and the current thermodynamic state of the atmosphere are connected through the physics of infrared radiation. In fact, each layer in the column of air directly overhead the instrument emits infrared radiation based on the local temperature and proportionally to the local absorption coefficient, which varies spectrally due to the chemical-physical properties of various trace gases like water vapor and carbon dioxide. The volume of air between each emitting layer and the observer at the ground, in turn, absorbs and scatters the downwelling emission, also based on the local absorption coefficient. The latter is the physical parameter that quantifies the opaqueness of a medium to incident radiation and is highly dependent on the wavenumber, $\tilde{\nu}$, of the radiation itself (Siegel, 1971). In general, more opaque wavenumber regions will allow only emission close to the observer to reach the ground-based spectrometer. Conversely, transparent wavenumber regions will let radiation emitted from higher altitudes be detected by the instrument. These properties are exploited to infer the vertical distribution of temperature profiles based on the spectral behavior of the radiance passively measured at the ground.

TROPoe utilizes a spectrally-resolved and extensively validated radiative transfer model (Turner et al., 2004; Clough et al., 2005; Mlawer and Turner, 2016) to simulate the spectral radiance that is associated with a given temperature profile. The model includes a detailed description of the physics of radiation and the molecular mechanisms that govern the absorption/emission at different wavenumbers. The main task of the thermodynamic retrieval algorithm is then to solve the inverse radiative transfer problem based on the observations, which is an ill-posed mathematical operation. The solution method for this challenging problem is described next.

https://doi.org/10.5194/wes-2025-198
Preprint. Discussion started: 15 October 2025

eawe european academy of wind energy
Open Access WIND ENERGY SCIENCE DISCUSSIONS

2.2 Fundamentals of TROPoe

Calculating the spectral radiance for a given temperature profile represents a complex but relatively established task; however, the inverse problem is significantly more complex. Unlike other remote sensing instruments like lidars and radars, the ASSIST is completely passive in the sense that it does not emit any electromagnetic pulse that could be used to perform ranging, for instance, based on the time of flight. Instead, it observes only the radiation at the ground, while the estimation of the associated temperature profiles is done in a purely mathematical way by inverting the radiative transfer problem, which is an integral equation. This can be seen as the impossible task of guessing the shape of a solid object by just looking at its shadow.

TROPoe uses optimal estimation techniques (Rodgers, 2000; Turner and Löhnert, 2014) that leverage the statistical information on the temperature profiles collected by previous radiosonde launches to constrain the problem and converge to a unique solution. Specifically, the mean and level-to-level covariance of temperature, T, and mixing ratio, r, at different heights, z, are compiled into the so-called prior. The use of optimal estimation not only facilitates the convergence of TROPoe to a realistic solution, but also provides as an output the posterior covariance, which quantifies the uncertainty of the retrieval. The embedded uncertainty quantification represents an advantage of TROPoe compared to regression or machine learning-based methods for temperature profiling. Full details of TROPoe are given in Turner and Löhnert (2014); Turner and Blumberg (2019).

The process just described is depicted in Fig. 1, and it is generally more complex and computationally expensive than other techniques used to observe atmospheric quantities using in-situ or remote sensing devices. However, physical-iterative retrieval frameworks like TROPoe have several advantages that more statistically-based retrieval methods do not (Maahn et al., 2020; Letizia et al., 2025), such as the cited uncertainty estimation, a broader generality, and easier troubleshooting. Understanding the limitations of temperature profiling is indeed crucial for an informed use of the data products. Therefore, the following section discusses the possible sources of uncertainty associated with our temperature profiling.

2.3 Sources of uncertainty

When discussing the accuracy in temperature profiles, it is important to distinguish between known and unknown uncertainties. The former are included in the posterior covariance generated by TROPoe, the latter are not. The known error can be expressed as (Rodgers, 2000):

$$\hat{x} - x = \overbrace{(A - I)(x - x_a)}^{\text{smoothing}} + \overbrace{G\epsilon}^{\text{noise}}, \tag{1}$$

where:

- $\hat{x}$ is the estimated state (i.e., estimated temperature profiles)
- x is the true state (i.e., real temperature profiles)
- I is the identity matrix
- A is the so-called averaging kernel or A-kernel, an important output of TROPoe

https://doi.org/10.5194/wes-2025-198
Preprint. Discussion started: 15 October 2025

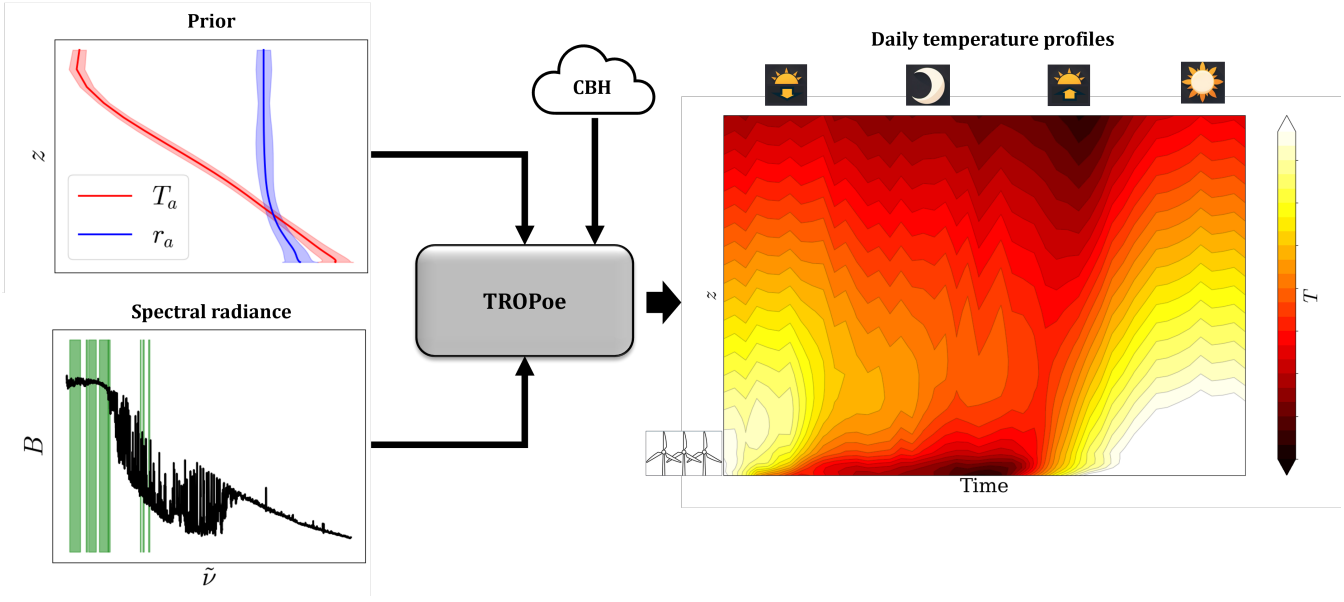

Figure 1. Workflow of temperature profiling. The green bands in the spectral radiance are those used for AWAKEN.

- G is the so-called gain matrix, an intermediate product of TROPoe
- ϵ is the noise on the observations (i.e., on the spectral radiance).

The known error is therefore the sum of the effect of smoothing and noise. The smoothing is a typical source of uncertainty in optimal estimation-based atmospheric sounding. The retrieved profiles are, in fact, a smoothed version of reality with a vertical resolution that is roughly equal to the height above the ground level. This makes temperature profiling more accurate close to the ground (where, for instance, wind turbines operate), and less accurate at the top of the boundary layer. In fact, sharp temperature inversions that typically occur at the top of the ABL are often significantly smoothed out. Smoothing is the result of incomplete information on the thermodynamic state in the spectral radiance that makes TROPoe partly reliant on the prior statistics. However, the smoothing error is predictable and included in the posterior uncertainty.

The error due to noise, instead, comes from random, zero-mean fluctuations on the observed spectral radiance due to imperfect hardware. Noise in the ASSIST is generally very small and is estimated in real-time by the instrument's processing software (Michaud-Belleau et al., 2025). The instrumental noise variance is included in TROPoe to calculate the posterior uncertainty of the solution.

Unknown uncertainties can be generally attributed to instrumental biases and an imperfect radiative model. Regarding the former, the 3σ bias in the spectral radiance is generally below 1% of the ambient black body emission (i.e., the highest emission typically observed in an atmospheric scene). This is ensured by online radiometric calibration, which was perfected throughout the 30-year-long AERI program (Knuteson et al., 2004a, b; Mlawer and Turner, 2016), and has been verified (Turner et al., 2025). These specifications translate into a 3σ bias in temperature of less than 1°C.

https://doi.org/10.5194/wes-2025-198
Preprint. Discussion started: 15 October 2025

eawe european academy of wind energy
Open Access WIND ENERGY SCIENCE DISCUSSIONS

However, the most insidious error comes from the imperfect description of the physics in the radiative transfer model. In fact, to make the model computationally efficient, TROPoe disregards some phenomena, such as atmospheric scattering. The physical constants in the model, for example, the spectral width of water vapor and carbon dioxide absorption lines, are also affected by uncertainty. An online estimation of the radiative transfer model error is possible, but not practically viable at the moment (Maahn et al., 2020).

Finally, prior radiosonde measurements used to constrain the calculation could be a source of bias if they are not representative of the observed climatology. This is relatively straightforward to diagnose (Maahn et al., 2020).

3 Results from pre-campaign tests

3.1 Overview

Before AWAKEN, the three NREL ASSISTs were deployed at the NREL Flatirons Campus close to Boulder, CO, for testing (Fig. 2). ASSIST 1 (Letizia, 2022b) and 2 (Letizia, 2022c) were co-located and operated for 97 days from May 18th to August 24th, 2022, providing an extensive record of observations that will be here used to assess the instrumental error (Section 3.2) and the total error (Section 3.3). Additionally, 24 days of temperature profiles from ASSIST 3 (Letizia, 2022a) are also available and will be occasionally used in Section 3.3. The 135-m M5 meteorological (met) mast (Clifton, 2014) is located on the North-East side of the campus and collected thermodynamic and kinematic atmospheric data at 1 Hz, which represents our main reference dataset. A second met mast, the 82-m M2 tower, is installed on the west side of the campus and was used as a redundant measurement point, as discussed in Section 3.3. A Vaisala CL51 ceilometer (Hamilton, 2022) was also deployed at that time, approximately 425 m northwest of the ASSISTs, providing CBH to TROPoe. As indicated in Fig. 2, several wind turbines are present on site and sporadically operated for research purposes. The local topography is characterized by a gentle $\sim 2\%$ W-E down slope, resulting in 7 m of difference in elevation between the ASSIST 1 and 2 and the reference met tower. In the following, temperature measurements will be compared based on the height above the local ground, thus assuming perfectly terrain-following temperature profiles. Neglecting terrain effect at the site is, in fact, common for instrument inter-comparisons (Wang et al., 2015; Letizia et al., 2024).

The climate at the site is typically semi-arid, with sunny conditions 70% of the daytime, which generally produces a markedly diurnal cycle of atmospheric stability. Wind conditions are significantly affected by the diurnal cycle, and also by the presence of the Rocky Mountains to the west that often channelize the flow, creating strong winds (Hamilton and Debnath, 2019). The data collected by the M5 met tower confirm these behaviors during the present campaign. In accordance with previous studies of the site (Aitken et al., 2014; Hamilton and Debnath, 2019), the atmospheric stability is classified based on the gradient Richardson number, Ri, evaluated between 3 and 122 m, using the ranges reported in Table 1. The hourly distribution of stability shows a clear daily cycle (Fig. 3a), also reflected in the daily-averaged temperature signals at different heights above the ground (Fig. 3b). The wind rose is also shown in Fig. 3c.

Temperature profiles were retrieved using TROPoe v0.12 (Turner, 2025), which ingested the spectral radiance from the ASSIST at selected bands as the main observations. The prior used to facilitate the convergence of TROPoe includes ensemble

https://doi.org/10.5194/wes-2025-198
Preprint. Discussion started: 15 October 2025

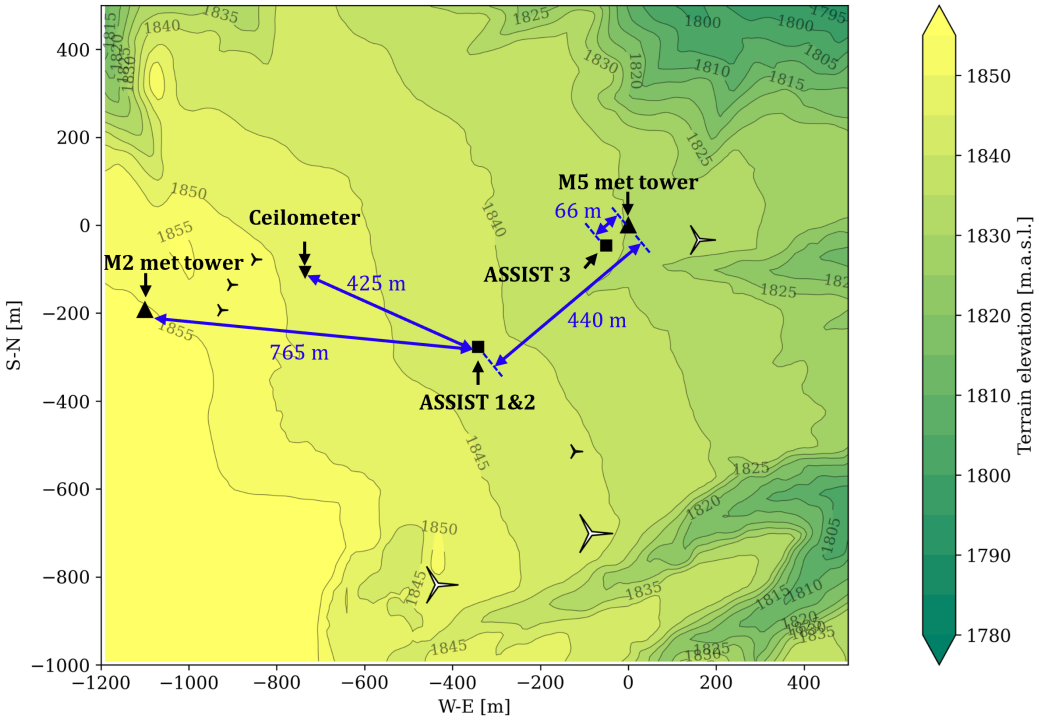

Figure 2. Map of the NREL Flatirons Campus in 2022. The size of the turbine rotors is to scale.

Ri range	Stability class	Symbol
≥ 0.25	Stable	S
$[0.03, 0.25)$	Neutral-stable	NS
$[-0.03, 0.03)$	Neutral	N
$[-0.25, -0.03)$	Neutral-unstable	NU
< -0.25	Unstable	U

Table 1. Stability classes based on the Richardson number calculated between 3 and 122 m.

means and level-to-level covariances of temperature and mixing ratio profiles from 1811 radiosonde launches in the Denver area. The lowest CBH from the ceilometer is also assimilated by TROPoe to enhance the accuracy of the solution in cloudy scenarios (Turner and Löhnert, 2014).

175 TROPoe profiles are quality-controlled by rejecting data above the base of optically thick clouds, with root-mean square between the observed and predicted radiance larger than RMSA>5, or with convergence parameter, $\gamma > 1$ (see Letizia et al. (2025) for details). Clouds detected when the TROPoe estimate for the liquid water path is less than 5 g m^{-2} are considered optically thin and thus bypassed. Table 2 reports the overall TROPoe temperature statistics for ASSIST 1 in terms of data availability after quality control, mean uncertainty (σ_T), mean vertical resolution (δz), and cumulative degrees of freedom (CDFs).

https://doi.org/10.5194/wes-2025-198
Preprint. Discussion started: 15 October 2025

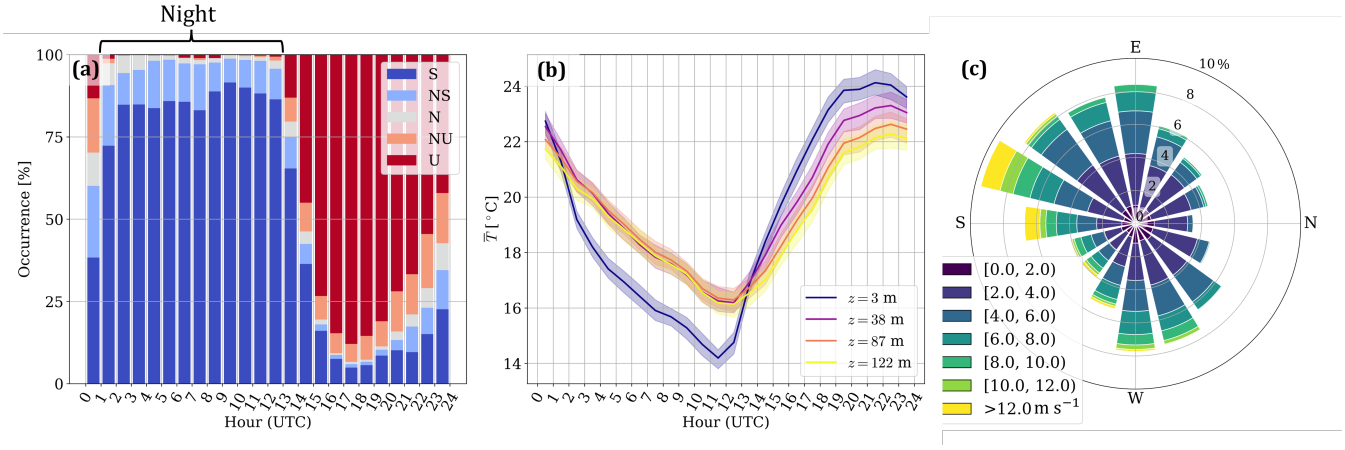

Figure 3. Climate statistics during the pre-AWAKEN campaign test from M5: occurrence of stability as a function of time of the day, based on the Richardson number between 3 and 122 m (S=stable, NS=neutral-stable, N=neutral, NU=neutral-stable, U=unstable) (a); daily-averaged temperature at different heights, where the shaded region represents the 95% confidence interval (b); wind rose at 74 m (c). Precipitation and wake events are excluded.

The latter is a measure of the information content below the selected height (see Turner and Löhnert (2014)). Uncertainty and vertical resolution increase with height, while most of the information content is confined close to the surface. This is a typical behavior of atmospheric sounding based on ground-based passive observations (Turner and Löhnert, 2021).

z [m]	Data availability [%]	σ_T [°C]	δz [m]	CDFs
10	90	0.08	28	0.95
100	90	0.21	168	1.94
1000	87	0.58	1589	3.42

Table 2. Mean statistics on the TROPoe temperature retrieval statistics of TROPoe temperature retrieval for ASSIST #1 based on 12,927 temperature profiles derived from data collected during the pre-campaign test.

Temperature profiles are generated every 10 minutes as a trade-off between temporal resolution and computational costs. To achieve this, TROPoe extracted the nearest in time spectral radiance collected by the ASSISTs at a sampling rate of ~ 14 s. The radiative transfer model is non-linear, so using high-frequency observation rather than, for instance, 10-minute-averaged ones, prevents the ingestion of non-realistic spectral radiances that can occur when averaging several sky scenes with different radiative properties. This is typical of scattered cloudy conditions. One drawback of using ASSIST data collected at the native sampling rate is that the noise is not averaged out, as it would occur by using time-averaged radiances. Therefore, the noise in the spectral radiances is removed through a Principal Component Analysis filter (Turner et al., 2006).

https://doi.org/10.5194/wes-2025-198
Preprint. Discussion started: 15 October 2025

eawe european academy of wind energy
Open Access WIND ENERGY SCIENCE DISCUSSIONS

Furthermore, the use of high-frequency data implies that the observed profiles include a significant turbulent contribution. To understand the behavior of turbulence at the site, we calculated the directional, daily-averaged, 10-minute second order moments of both temperature and wind speed in the form of temperature standard deviation ($\sqrt{\overline{T'^2}}$) and turbulence intensity (TI) from 1-Hz met tower data (Fig. 4). The inner circle of the polar plot corresponds to nighttime, while the outer one corresponds to daytime. In other words, radial variations of the quantity indicate a diurnal cycle, and departures from axial symmetry represent the effects of wind direction. Both $\sqrt{\overline{T'^2}}$ and TI show the expected diurnal cycle with larger fluctuations during the day (i.e., unstable conditions), although directional effects are also important. In particular, the temperature standard deviation plot at 3 m (Fig. 4a) reveals consistently large fluctuations during night hours and especially for WSW winds. A TI peak for the same time/direction is not evident. The fluctuations occurred with periods of several minutes and are confined close to the surface, which is reminiscent of the gravity wave events documented by Sun et al. (2015). Further investigation is beyond the scope of this work; however, the effect of turbulent fluctuations on the temperature differences observed at different sites is discussed in Section 3.3.

3.2 Exploring instrumental error: side-by-side test

In this section, we discuss the temperature differences observed between the co-located ASSIST 1 and 2. The comparison is important to assess the instrumental error. In fact, subtracting the temperature estimated by TROPoe for the two independent instruments leads to a theoretically perfect cancellation of the smoothing and radiative model errors in TROPoe. What is left is the effect of bias in the measurements (which would translate into a mean temperature difference) and noise (which would translate into a random, zero-mean temperature difference). By applying the general TROPoe posterior uncertainty (Eq. 1) to the temperature difference, we get:

$$\Delta\hat{T} = \hat{T}_2 - \hat{T}_1 = G(\epsilon_2 - \epsilon_1), \tag{2}$$

where we have taken advantage of the equivalent TROPoe settings for both units to eliminate the smoothing error and isolate a common G matrix. Since instrumental noise, ϵ, is assumed to have zero mean, the theoretical mean of $\Delta\hat{T}$ is 0. We can safely assume negligible correlation between the instrumental noise of independent units, so that the predicted covariance of the temperature differences is:

$$S_{\Delta\hat{T}} = G(S_{\epsilon,1} + S_{\epsilon,2})G^T, \tag{3}$$

where S_ϵ is the covariance of the instrumental noise for each instrument, a nearly diagonal matrix that is estimated by the ASSIST online. The instrument-to-instrument error standard deviation that we will use next, $\sigma_{\Delta\hat{T}}$, is then simply the square root of the diagonal $S_{\Delta\hat{T}}$.

To test the validity of this framework, we retrieved more than 10,000 temperature profiles through TROPoe from both ASSISTs and calculated statistics of the temperature difference, $\Delta\hat{T}$, at each height up to 2000 m above ground level. The results are shown in Fig. 5 in terms of bias (i.e., mean difference) (a), Root Mean Square (RMS) of temperature difference (b), and probability of exceeding the 95% TROPoe confidence interval (c.i.) predicted by TROPoe (c) as a function of height.

https://doi.org/10.5194/wes-2025-198
Preprint. Discussion started: 15 October 2025

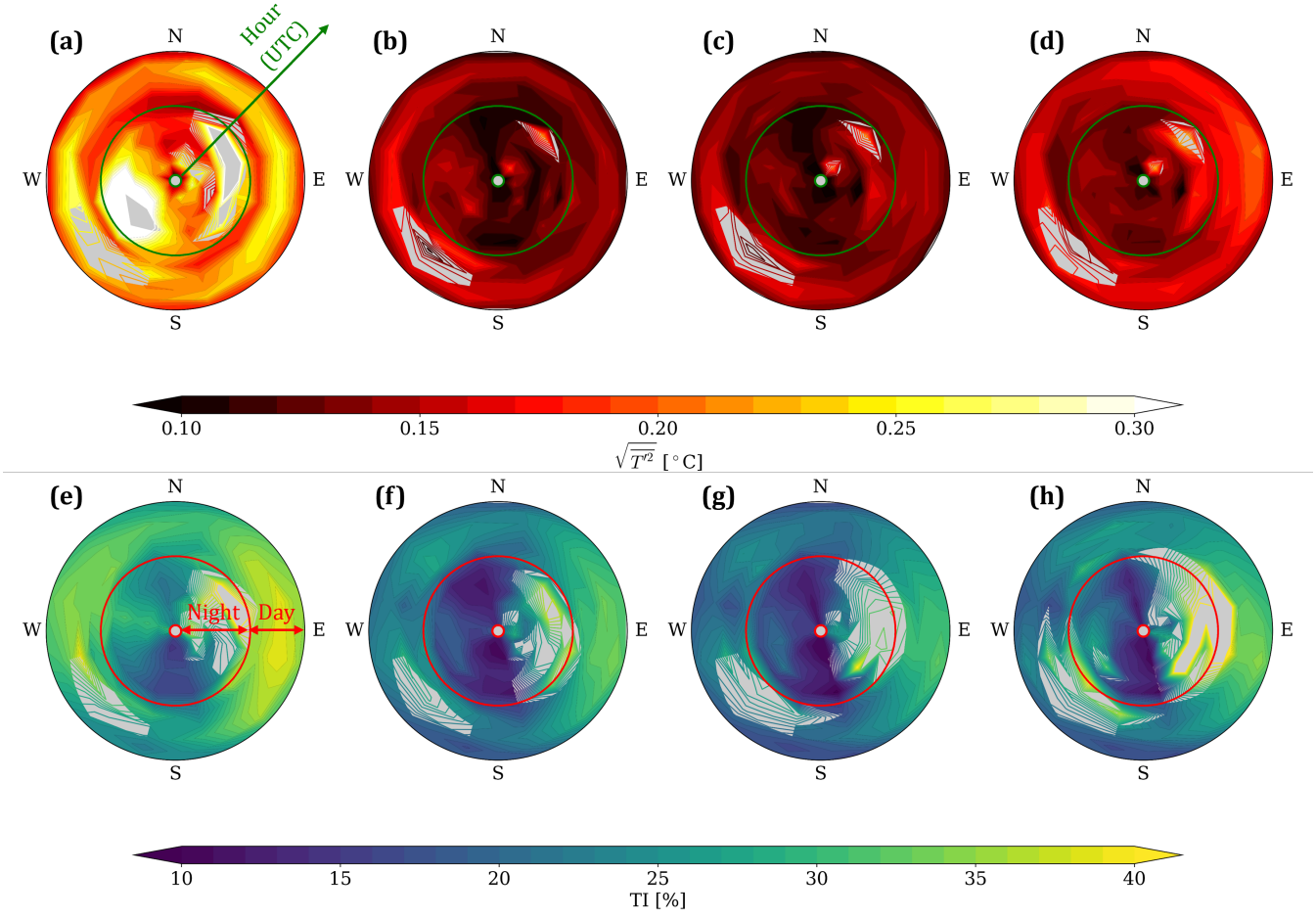

Figure 4. Directional, daily-averaged standard deviation of temperature (a-d) and turbulence intensity (TI) (e-h) at different heights: 3 m (a,e); 38 m (b,f); 87 m (c,g); 122 m (d,h). The areas with transparent fills have a 95% confidence interval larger than 0.1°C or 10% for temperature standard deviation and TI, respectively.

The bias is extremely small (< 0.02°C) and practically irrelevant for most applications, which validates the assumption of negligible instrumental bias. The RMS of $\Delta\hat{T}$ is below 0.3°C, and exhibits a gradual monotonic trend with height, except for a peak close to the surface; these bias and RMS results agree with Turner et al. (2025). The error model based on TROPoe ($\sigma_{\Delta\hat{T}}$ from Eq. 3 and red line in the figure) is in fair agreement with the observations (black line). The trend as a function of height is well-captured, but the theory underestimates the error below 100 m and overestimates it above. This discrepancy may come from either an imperfect estimation of the noise from the ASSIST and/or noise that violates the assumption of Gaussianity used

https://doi.org/10.5194/wes-2025-198
Preprint. Discussion started: 15 October 2025

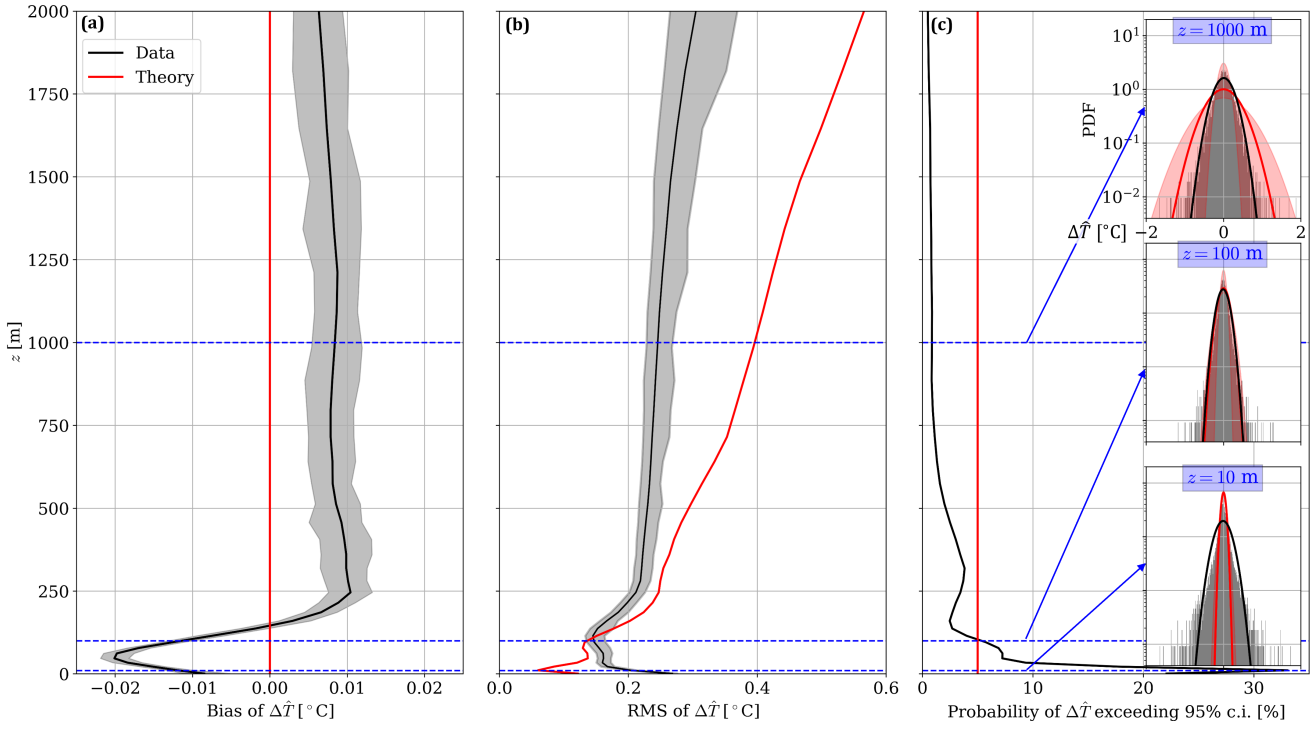

Figure 5. Vertical profiles of statistics of temperature differences between ASSISTs 1 and 2, $\Delta\hat{T}$: mean (a); RMS (b); probability of exceeding the 95% TROPoe c.i. (c). The PDFs of temperature difference at selected heights are provided as insets with equal axes in (c). The shaded area in (a) and (b) represents the 95% statistical c.i., while in (c) represents the PDFs with the largest and smallest TROPoe uncertainty.

by TROPoe. To further explore the ability of theory to predict the distribution of $\Delta\hat{T}$, we plot the probability of $\Delta\hat{T}$ exceeding the 95% c.i. obtained from Eq. 3 and assuming a Gaussian distribution (i.e., the probability that $\Delta\hat{T} \notin \pm 1.96\ \sigma_{\Delta\hat{T}}$). Close to the ground, where theory underestimates the standard deviation of $\Delta\hat{T}$, there is up to 30% probability of finding a value outside the c.i., which is significantly larger than the expected 5%. The corresponding real histogram (gray) and Gaussian fit (black line) of the probability density function (PDF) at $z = 10$ m shows a leptokurtic behavior of $\Delta\hat{T}$ not captured by TROPoe theory (red line) that always assumes Gaussianity. The model predicts fairly the bulk of variability around 0, but the likelihood of large and extreme $\Delta\hat{T}$ events is clearly underpredicted at this height. Moving to $z = 1000$, we see an opposite behavior: the mean uncertainty estimation by Eq. 3 is too conservative, with real values more peaked around 0 than predicted. These opposite trends cancel out at $z = 100$, where the prediction of TROPoe is spot on.

The main takeaways of this section are:

1. TROPoe temperature retrievals from two identical ASSISTs show negligible bias and an RMS of < 0.3°C of difference, the latter being predicted fairly well by TROPoe uncertainty product.

https://doi.org/10.5194/wes-2025-198
Preprint. Discussion started: 15 October 2025

eawe european academy of wind energy
Open Access WIND ENERGY SCIENCE DISCUSSIONS

2. Random uncertainty from both the met data and TROPoe estimate spikes and departs from Gaussianity in the lowest 20 m, with TROPoe slightly underpredicting its magnitude.

3.3 Quantification of total error near the surface: comparison with met tower

Now that the instrument-to-instrument error has been documented and proven to be negligibly biased and predictable for common applications, in this section, we focus on a more comprehensive characterization of the total error. This includes contributions from smoothing, forward model, and prior, in addition to the error due to instrumental noise. The total error of the temperature profiles is quantified through a comparison with the temperature readings of the Resistance Temperature Detector (RTD) probes installed on the M5 tower. Specifically, the temperature profile is reconstructed by combining the absolute temperature measured at 3 m and differential temperature measurements between 3 and 38, 38 and 87, and 87 and 122 m. The use of differential temperature measurement is advantageous because it maximizes the sensitivity of the probe, allowing the gain applied to the raw signal and thus error amplification to be reduced. Resulting temperatures at 4 heights (3, 38, 87, and 122 m) have a reported uncertainty of 0.1°C (St.Martin et al., 2016) which we interpret as a 1σ value. Temperature probes are housed inside a radiation shield with active ventilation capabilities. However, during this campaign, some ventilation fans were not active. Therefore, the temperature readings from the unaspirated sensors on M5 were corrected for radiative error using the method by Nakamura and Mahrt (2005) and the M2 tower (which was aspirated) as a reference (see Appendix A for details).

The high-frequency temperature time series from M5 collected at 1 Hz are downsampled through a rolling average to match the sampling rate of the ASSIST (14 seconds), then linearly interpolated in time on the TROPoe time grid (one profile every 10 minutes). TROPoe data is interpolated linearly in z to match the met tower heights. No attempt is made to time-shift either dataset to account for the advection across the 440-m distance between the two instruments, mainly because the dataset also encompasses wind direction where the two instruments are not aligned with the wind. Differences in temperatures due to spatial decorrelation of turbulent thermal structures in space are, therefore, an additional source of random "representativeness" error in the data and will be discussed separately.

Figure 6 shows three illustrative time series from both met probes and TROPoe at all available heights. The first was recorded during the passage of a cold front that caused a drop in temperature of about 15°C in 20 minutes. TROPoe detects the drastic temperature change with excellent agreement when compared to M5, indicating the ability of our ground-based passive temperature profiling method to work robustly in dynamic atmospheric environments.

The second time series corresponds to an overcast event (see cloud height on the top panel) that disrupted the typical diurnal thermal cycle. Discrepancies during the coldest hours with low clouds are within a fraction of a degree. This is an early indication that temperature estimates close to the surface are minimally affected by clouds that, as we mentioned, represent a major challenge for temperature profiling using passive spectral infrared methods. The accuracy of TROPoe in this case is remarkable, considering that low clouds have a powerful emission in the infrared region that may have obscured the thermodynamic information.

https://doi.org/10.5194/wes-2025-198
Preprint. Discussion started: 15 October 2025

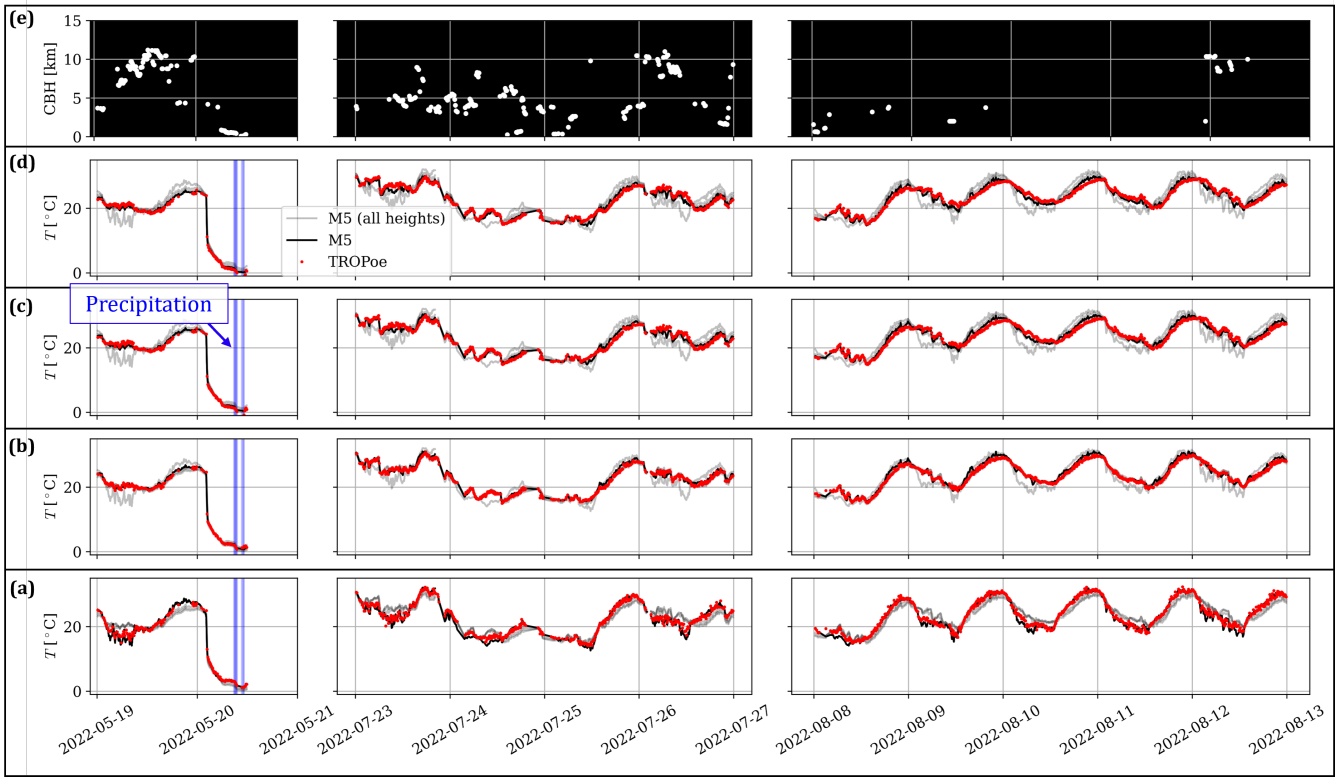

Figure 6. Selected time series of temperature from M5 and TROPoe at different heights: 3 m (a); 38 m (b); 87 m (c); 122 m (d). The CBH is shown in (e). The light gray lines represent the met tower observations at all heights and are superposed to evaluate the ability of TROPoe to match vertical temperature gradients.

The third and possibly more insightful time series corresponds to a sequence of hot, clear-sky days. Here, the differences between TROPoe and the met tower appear more systematic, with a consistent warm bias at night and a cold bias during the day, the latter being less evident at the lowest height.

Figure 7 offers a more quantitative insight into the temperature differences over the entire dataset. Linear fits at different heights (Fig. 7 a,b,c,d) show R^2 above 0.98, very small bias, RMS $< 1°$C, and, interestingly, a slope slightly less than one at all heights. Rather than being a statistical artifact (e.g., slope dilution (Frost and Thompson, 2000)), this is more likely an indication that either TROPoe is underestimating the diurnal variation of temperature compared to M5, or the effect of a residual error in the correction of the radiative error of M5 (see Appendix A). This is also consistent with the diurnal bias seen in Fig. 6.

Before digging into the possible cause of the observed discrepancies, an important question is: "How well does the TROPoe posterior uncertainty product capture the observed differences?". To this aim, we visualize histograms of temperature differences at all heights (Fig. 7 e,f,g,h) and superpose the expected error Gaussian PDF obtained by combining TROPoe+M5 uncertainties. The real PDF of ΔT (gray bars) is minimally biased and arguably Gaussian, especially above 3 m (the black

https://doi.org/10.5194/wes-2025-198
Preprint. Discussion started: 15 October 2025

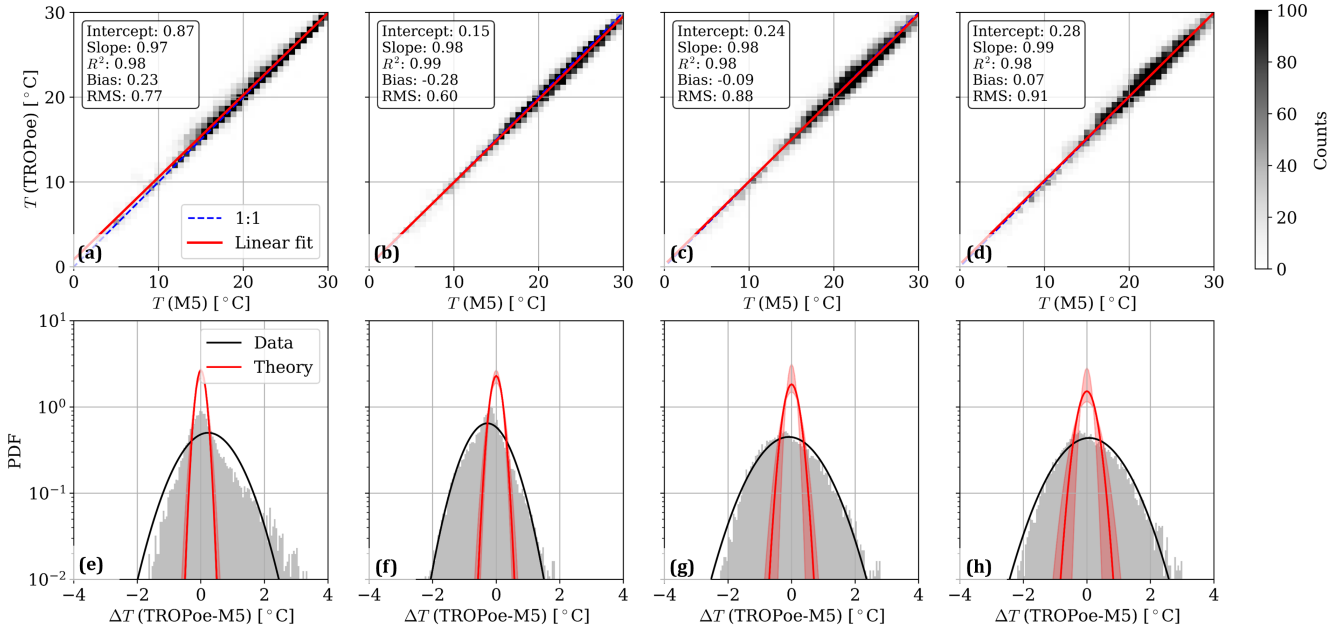

Figure 7. Statistical quantification of the temperature differences between TROPoe and M5 at different heights: (a-d) linear regression; (e-h) histograms, where the shaded red area indicates the error PDF using the minimum and maximum combined TROPoe+M5 uncertainty. 3 m (a,e); 38 m (b,f); 87 m (c,g); 122 m (d,h).

line is the Gaussian fit). However, the standard deviation is 3 to 5 times larger than the predicted uncertainty, indicating an additional source of error in the dataset. Having excluded the instrumental bias or an under-predicted noise in Section 3.2, we are left with two main candidate sources of uncertainty: the spatial separation between the ASSIST location and M5 and the radiative transfer model (the prior was confirmed to match the observed climatology and thus ruled out as a source of uncertainty).

The error due to spatial separation is associated with the spatial decorrelation of turbulence. Its magnitude can be estimated through the temperature structure function, defined as the variance of the temperature difference as a function of space. For an ergodic, horizontally homogeneous field, this reads:

$$D_T(\mathbf{r}, z) = \overline{(T(\mathbf{x}) - T(\mathbf{x}+\mathbf{r}))^2}, \tag{4}$$

where the overbar indicates time average (in our case, over the standard 10-minute window), $\mathbf{r}$ is the separation along a certain direction, and $\mathbf{x}$ is a reference point in space. A direct application of Eq. 4 would require the placement of multiple sensors at different locations. For the sake of simplicity, it is customary to instead use Taylor's frozen turbulence hypothesis (Taylor, 1938), which de Silva et al. (2015) showed to work well up to separation distances as large as the boundary layer height in neutral conditions. Han and Zhang (2022) showed that Taylor's hypothesis fails to replicate spatial structure temperature functions under unstable conditions and for short separations, while it works well in other conditions. Here we use Taylor's

https://doi.org/10.5194/wes-2025-198
Preprint. Discussion started: 15 October 2025

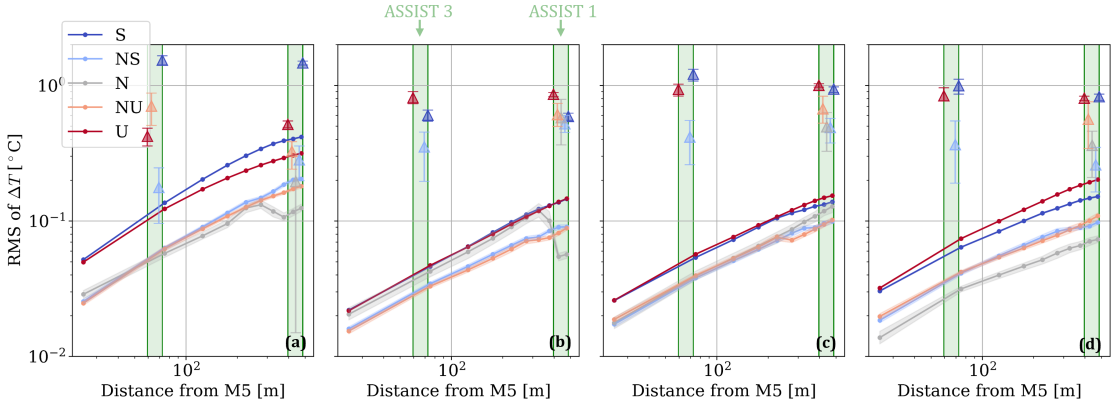

Figure 8. Estimated standard deviation due to spatial separation (lines) as a function of distance from M5 and stability at different heights, and corresponding RMS of temperature difference from ASSISTs 1 and 3 (triangles). Known TROPoe and met tower uncertainty has been removed from the RMS to isolate the residual component. 3 m (a); 38 m (b); 87 m (c); 122 m (d).

hypothesis to calculate the structure function based on temperature time series from the met tower up to separations of 440 m in all atmospheric conditions, which, based on the cited references, should represent an acceptable approximation of Eq. 4 for most of the cases. To maximize realism in the estimation of the spatial error between TROPoe and the met tower, we calculate the structure function of the temperature data downsampled to the ASSIST sampling rate of 14 s. Furthermore, we restrict the analysis to cases where the ASSIST and the met tower are aligned within 20° from the mean wind direction and to TI values smaller than 50% (Stull, 1988).

Figure 8 shows the standard deviation of the temperature differences based on the (square-rooted) time-based structure function at different heights and stabilities. The choice to cluster data in this function is inspired by the classical scaling of structure functions (Wyngaard et al., 1971; Wyngaard, 1973), which relates this statistical parameter mainly to stability and height. The structure function is seen to generally decrease with height and increase in unstable conditions, where more turbulence is expected. In our dataset, it also increases moving from neutral to stable, which is likely connected to the nighttime temperature oscillations whose signature appears in Fig. 4.

On the same figure, we report the residual RMS of temperature difference TROPoe vs. M5 after subtracting the known TROPoe+M5 uncertainty for ASSIST 1 (placed 440 m away from M5) and ASSIST 3 (placed 66 m away). If spatial variability were the only cause of the residual discrepancy, we would expect a match with the value estimated from the structure function at the corresponding distance, height, and stability. Although some trends do match (the highest RMS occur in stable and unstable conditions), the residual variability of ΔT far exceeds the estimated spatial component for most of the bins. An even stronger piece of evidence that the discrepancies between TROPoe and met are not only turbulence-driven is that the error does not decrease moving from ASSIST 1 (440 m away) to ASSIST 3 (only 66 m away). The fact that some additional source of uncertainty other than turbulence is contributing to fatten the PDF of ΔT is also suggested by the cyclical (thus not random, as turbulence would be) difference observed in Fig. 6 for clear-sky conditions.

https://doi.org/10.5194/wes-2025-198
Preprint. Discussion started: 15 October 2025

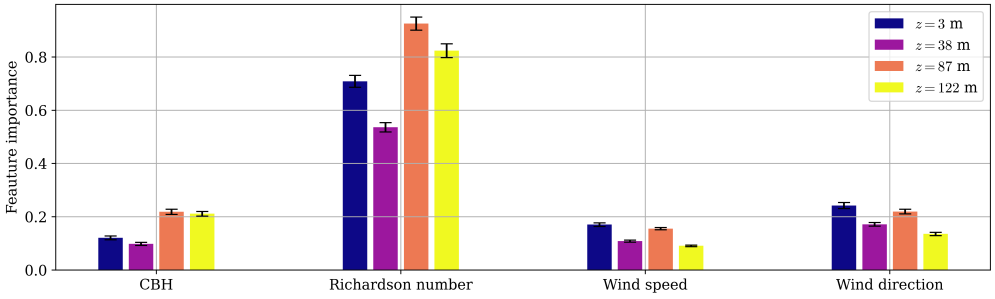

Figure 9. Random forest permutation feature importance of several atmospheric parameters as a descriptor of the temperature difference between TROPoe and M5.

After ruling out spatial variability as the only contributor to the temperature difference, we focus on describing the residual errors as a function of the atmospheric conditions. An objective way to assess the relevance of a set of inputs in describing a target parameter is the importance ranking through random forest permutations. We apply the framework described in Letizia et al. (2024) to the description of ΔT as a function of the atmospheric quantities in Fig. 9 for separate heights. The Richardson number (viz., stability) emerges as the most important parameter that describes the temperature differences. This confirms that the diurnal error pattern seen above is ubiquitous in the dataset.

To understand the magnitude of what appears to be a stability-dependent bias, we evaluate mean temperature profiles from TROPoe, M5, and M2 at the native heights for the different stability classes. Care has been taken to ensure that only periods when all three sources are available are included. Figure 10 shows the mean profiles, along with their 95% statistical c.i. The stability-dependent bias between TROPoe and M5 is more severe at higher z and for unstable and stable conditions. Neutral and near-neutral conditions show a bias that is within the statistical uncertainty. Compelling evidence that the observed difference is an actual bias and not an instrumental error from the met sensors or the effect of persistent thermal inhomogeneity is the excellent agreement between M5 and M2. To sum up, the present analysis highlights a stability-dependent bias that is always less than $1°$C and is mostly positive in stable conditions (TROPoe warmer than met towers) and negative during unstable conditions (TROPoe colder than met towers, except very close to the ground). Differences of this magnitude are similar to what was reported by previous studies (Blumberg et al., 2015; Klein et al., 2015; Bianco et al., 2024).

To conclude this section, we discuss the accuracy of temperature profiling in capturing vertical temperature gradients and hence the static stability of the surface layer. We first look at the linear regression between the vertical temperature gradient, $\Delta T \Delta z^{-1}$, evaluated from M5 vs. TROPoe at height pairs (Fig. 11). The highest agreement is observed for the combination of heights that result in larger gradients (i.e., close to the ground or for large vertical spacing), with R^2 values of 0.88. The agreement is slightly worse than what was reported for the LABLE experiment (Klein et al., 2015), although that study only included temperature gradients in the $\pm 0.01°$C m^{-1} range and had a smaller distance between the thermodynamic profiler and the reference instrument (the radiosonde launch station was 300 m away from the spectrometer). Poorer scores occur for

https://doi.org/10.5194/wes-2025-198
Preprint. Discussion started: 15 October 2025

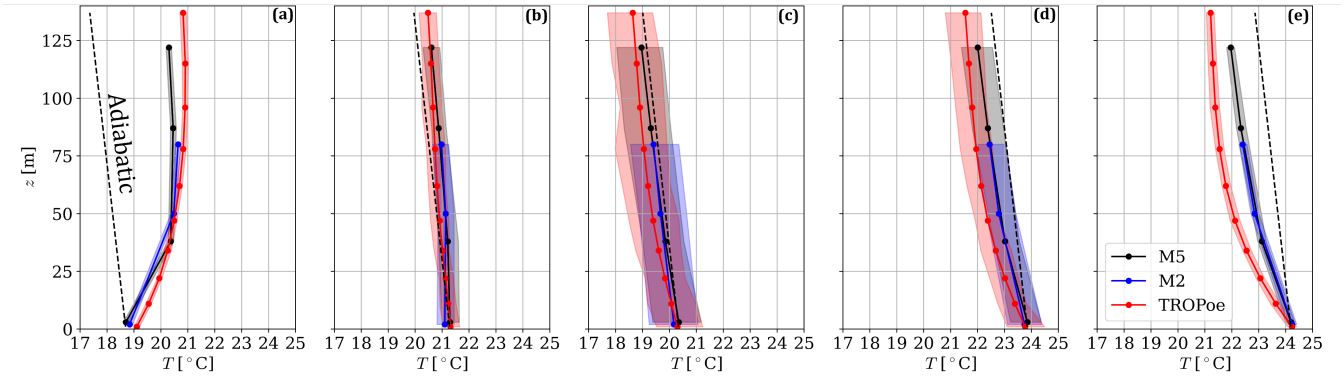

Figure 10. Mean temperature profiles for different stabilities: 6112 stable profiles (a); 862 neutral-stable profiles (b); 210 neutral profiles (c); 394 neutral-unstable profiles (d); 3314 unstable profiles (e).

height combinations where $\Delta T \Delta z^{-1}$ is small, which is expected for a constant level of random error or unexplained variance between the two variables. Also, at short vertical separations, the finite vertical resolution of the TROPoe grid begins to play a significant role.

We finally assess the difference in Ri-based stability classification when using M5 vs. TROPoe data. The Richardson number from TROPoe uses temperature and moisture content from TROPoe, while wind gradients are still necessarily from M5. Table 3 shows, for each stability class defined from the Richardson number using M5, the percentage distribution of stability classes derived from the Richardson number using TROPoe. Both Ri values are evaluated between 3 m and 122 m. This contingency table shows good agreement for the stable and unstable classes (83% and 97% hits, respectively). More discrepancies are observed for neutral and near-neutral conditions. These classes are also the narrowest in terms of Ri range and those with the lowest occurrence, thus more sensitive to differences in lapse rate. TROPoe is shown to have an unstable bias compared to M5. For instance, 11% of unstable occurrences according to M5 are identified as stable by TROPoe, which is consistent with the cold bias at 122 m seen in Fig. 10e. An imperfect removal of the overheating (Appendix A) due to solar radiation (the probe at 122 m is not aspirated) may also have contributed to the apparent unstable bias.

M5 \ TROPoe	S	NS	N	NU	U
S	83	4	0	0	11
NS	7	47	11	13	19
N	0	3	28	33	33
NU	0	1	1	28	68
U	0	0	0	1	97

Table 3. Percentage contingency table of stability classification based on Richardson number from either M5 (rows) and TROPoe (columns).

https://doi.org/10.5194/wes-2025-198
Preprint. Discussion started: 15 October 2025

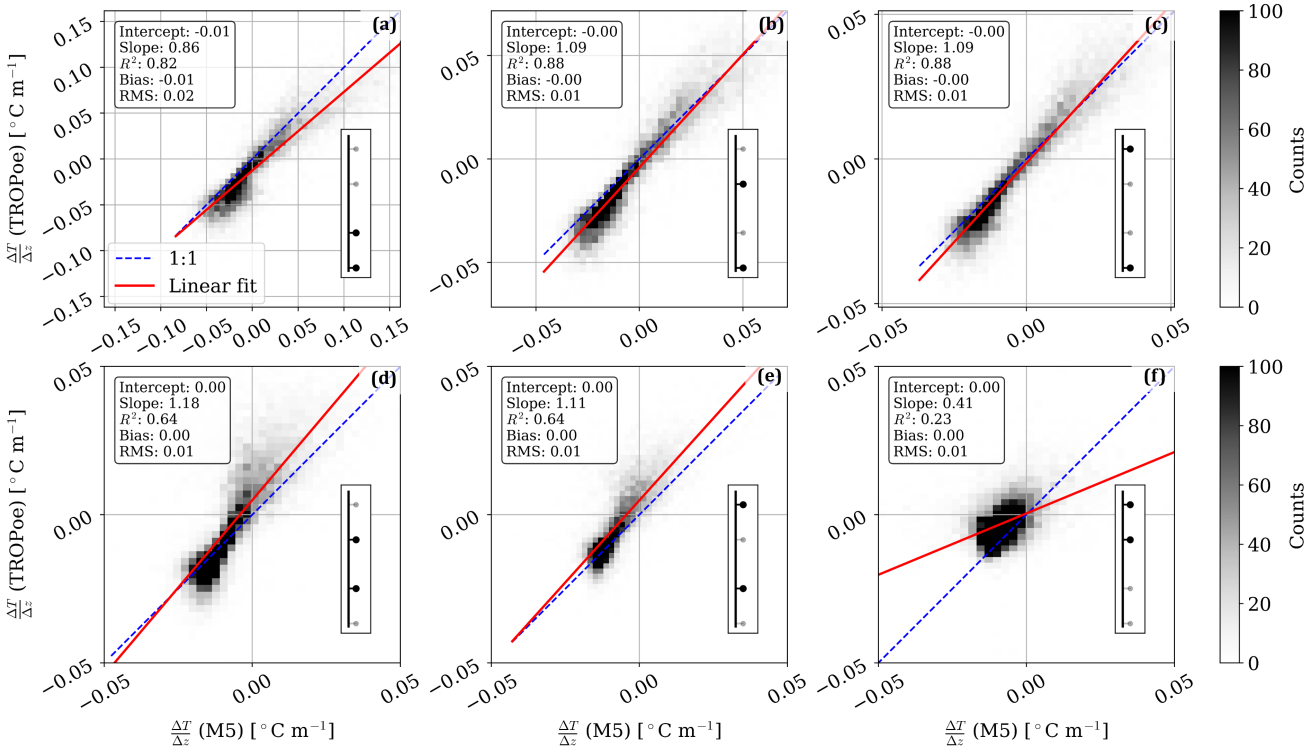

Figure 11. Linear regression between vertical temperature gradients from different height pairs: 3 and 38 m (a); 3 and 87 m (b); 3 and 122 m (c); 38 and 87 m (d); 38 and 122 m (e) 87, and 122 m (f).

The main takeaways of this section can be summarized as follows:

1. ASSIST+TROPoe performs satisfactorily at all the heights and conditions we tested for what could be considered general wind energy and meteorological applications, with an overall RMS of temperature difference with the met tower of less than 1°C and negligible overall bias.

2. The RMS of temperature differences could not be fully explained in terms of TROPoe and met tower uncertainty estimates and spatial decorrelation of thermal turbulence.

3. We identified a stability-dependent bias of less than 1°C that deserves further investigation.

4. ASSIST+TROPoe is confirmed to be remarkably accurate in identifying static stability of the surface layer, particularly for very stable and unstable conditions.

https://doi.org/10.5194/wes-2025-198
Preprint. Discussion started: 15 October 2025

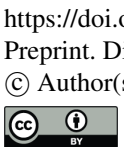

eawe european academy of wind energy
Open Access WIND ENERGY SCIENCE DISCUSSIONS

4 Results from AWAKEN

4.1 Overview

The AWAKEN experiment is a multi-institutional experimental campaign with the goal of investigating the interactions between the atmospheric boundary layer and land-based wind plants. It took place from 2023 to 2025 in northern Oklahoma, U.S. The reader is referred to Moriarty et al. (2024) and references therein for more details regarding the instrument layout and science goals.

Temperature profiling was an essential asset at AWAKEN and used the network of sensors shown in Fig. 12. This included three ASSISTs (South, Middle, and North) strategically placed to capture atmospheric conditions throughout the experimental domain. Each ASSIST was co-located with a surface met station (Goldberg, 2023e, f, g). Additional temperature profiling was conducted through radiosondes launched from the north-most site (Keeler et al., 2023).

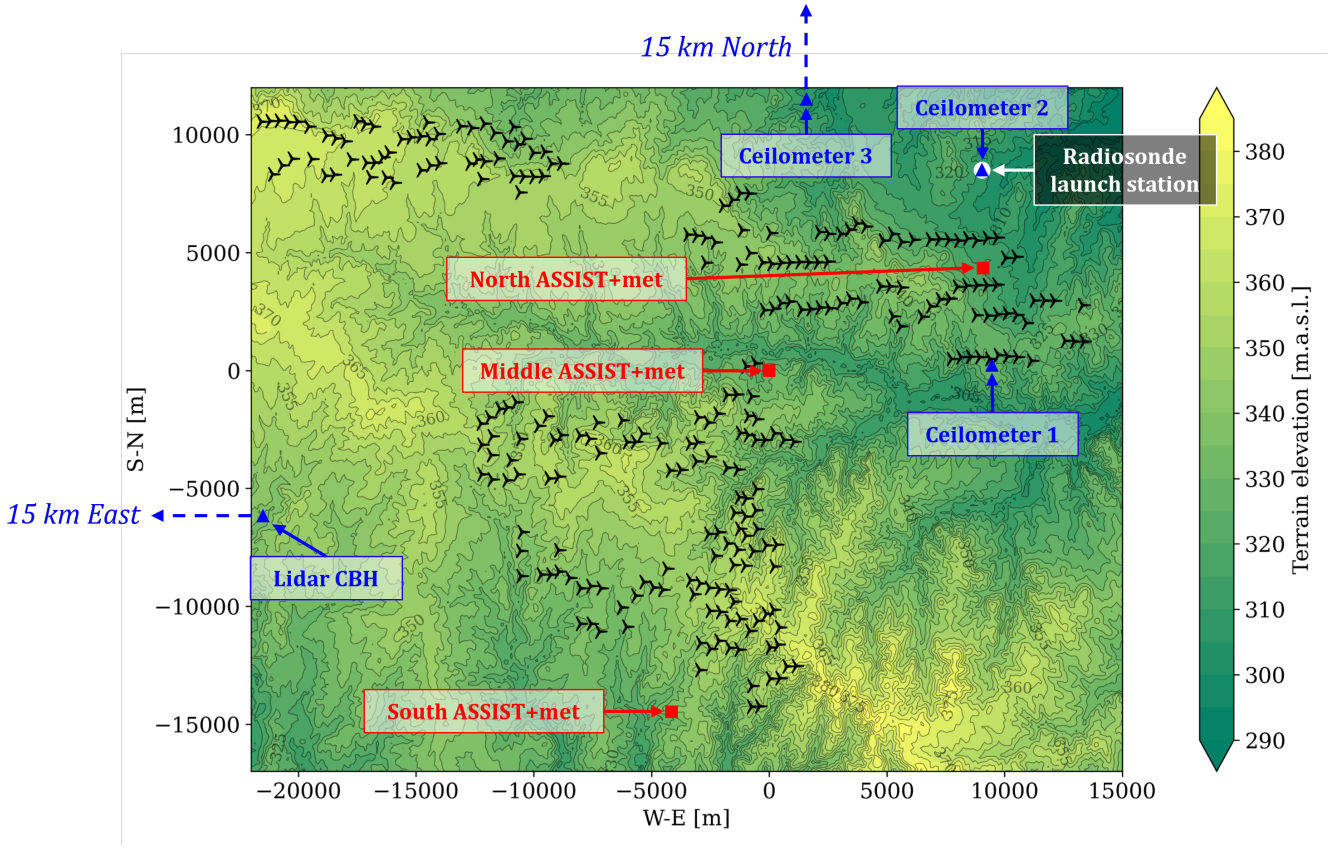

Figure 12. Map of the instruments used for temperature profiling and wind turbines at AWAKEN.

TROPoe was run with the same setup described in Section 3.1 and using a CBH from the three ceilometers (Hamilton, 2023; Zhang et al., 2023b, a) plus the lidar (Shippert et al., 2023) indicated on the map in blue. To account for the spatial variability of

https://doi.org/10.5194/wes-2025-198
Preprint. Discussion started: 15 October 2025

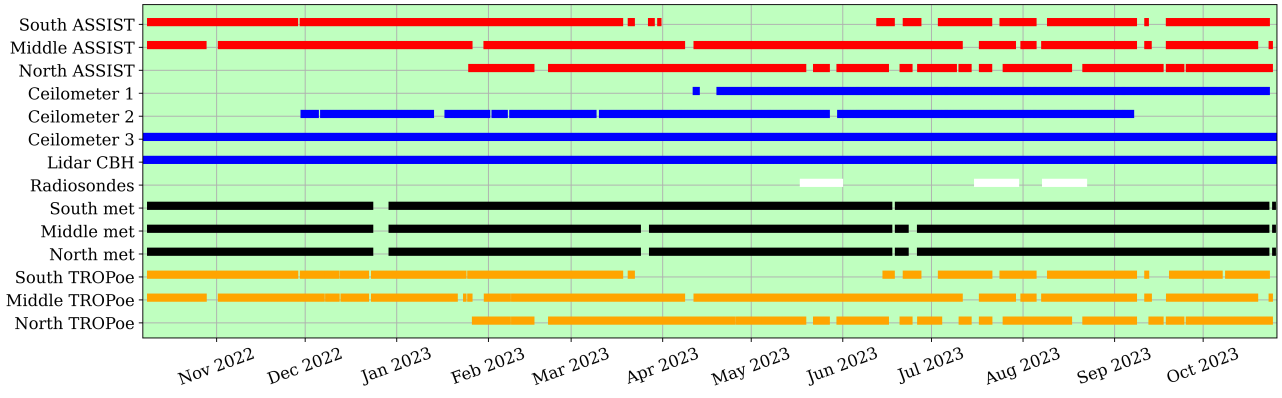

Figure 13. Data availability at AWAKEN.

cloud cover, the CBH for each ASSIST site is estimated as the average CBH from all available sources weighted by the inverse of the respective distance. The data availability of all input instruments and TROPoe retrievals is shown in Fig. 13. Overall, roughly one year of temperature profiles is available from all combined sites.

4.2 Quantification of error in whole ABL: comparison with radiosondes

The goal of this section is to quantify TROPoe's total error and the accuracy of the uncertainty estimate across the ABL. To this aim, we compare TROPoe retrievals at the North site with observations from radiosondes at AWAKEN. Radiosondes were launched in different phases from May 17 to August 22, 2022, at site H. The radiosonde model is the Vaisala RS-90 with an accuracy of temperature measurement of $0.15°C$ (Holdridge, 2020). The nominal schedule included 5 launches at 02:30, 05:30, 08:30, 11:30, and 23:30 UTC aimed at probing the nocturnal ABL. Out of the 198 available radiosonde launches, 116 have concurrent TROPoe retrievals and are used in this analysis. The comparison is carried out vs. radiosonde profiles downsampled at the ASSISTs sampling rate (14 s), both at the native resolution vertical and also on "TROPoe-smoothed" as done by (Blumberg et al., 2017). It can be proven (Letizia et al., 2025) that smoothing high-resolution profiles using TROPoe averaging kernel and prior theoretically eliminates the smoothing error and isolates the noise contribution.

All profiles and error statistics are shown in Fig. 14. The bias (Fig. 14a) peaks at the surface, where it reaches the modest value of $0.2°C$, which is smaller than what reported by previous similar studies (Blumberg et al., 2015; Klein et al., 2015; Blumberg et al., 2017; Turner and Blumberg, 2019; Turner and Löhnert, 2021). By looking at the temperature difference map in Fig. 14e, it appears that the cold bias close to the surface is due to persistent patches of negative temperature differences in the lowest 100 m associated with positive difference aloft that occurred for specific launches. Finally, smoothing the radiosonde profiles has little impact on bias.

The RMS of temperature difference (continuous black line in Fig. 14b) shows a peak at the surface ($0.9°C$) and a monotonic positive trend above 100 m. Values of the RMS in the range of heights considered are in line with the several references

https://doi.org/10.5194/wes-2025-198
Preprint. Discussion started: 15 October 2025

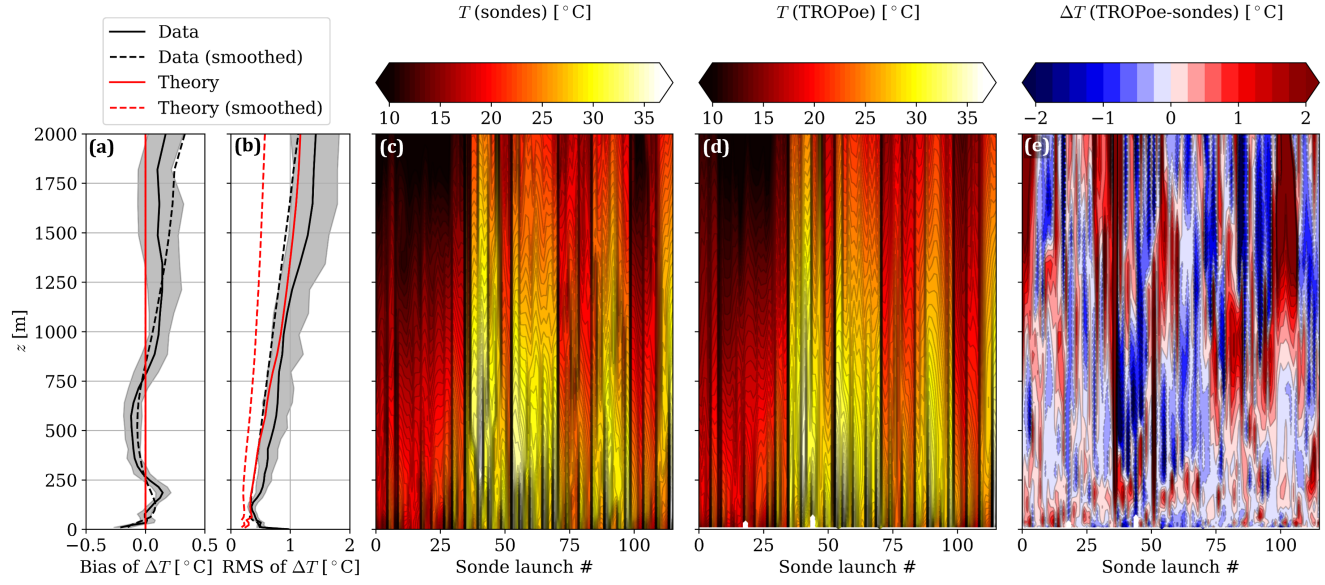

Figure 14. Vertical profiles of statistics of temperature differences between TROPoe at North site and radiosondes, ΔT: mean (a), RMS (b); all temperature profiles from radiosondes; (c) all temperature profiles from TROPoe at the North site (d); all temperature differences (e). Shaded areas in (a) and (b) correspond to the 95% c.i. of the statistics for unsmoothed profiles.

(Blumberg et al., 2015; Klein et al., 2015; Turner and Blumberg, 2019), except for the high value at the surface. This high RMS close to the ground is also due to the bias just discussed. The TROPoe total uncertainty estimate (continuous red line in Fig. 14b) amplified with the radiosonde (small) uncertainty captures remarkably well the trend of RMS above 100 m, although with an average 20% underestimation. This may be due to the effect of spatial decorrelation at the distance between the two instruments (4 km at the ground). RMS difference with smoothed radiosonde profiles (dashed black line in Fig. 14b) is expectedly lower than the total RMS due to the removal of the smoothing error, with TROPoe's noise-only+radiosonde uncertainty estimate being off by 40 %, in part due to the persistent bias, which is not smoothed out.

The presence of a persistent temperature anomaly at heights where wind turbines operate at AWAKEN led to the hypothesis that the observed bias could be caused by wake effects. Turbine wakes are known to generate turbulence that warms up the air below the rotor height and cools down the region above it (Wu et al., 2023) by diminishing the lapse rate in stable conditions. What we see in Fig. 14e, especially for launches #25 to #75, is compatible with wake effects affecting disproportionally more the radiosonde. The launch site is indeed downstream of the North site where the ASSIST operates (based on the prevalent wind direction), and therefore in the wake of more turbines.

Early evidence that wake effects may have played a role is provided in Fig. 15 that shows the temperature difference TROPoe-sondes averaged from the ground to wind turbine hub height as a function of mean wind direction and wind speed in the turbine layer. The sign of the temperature difference is highly dependent on wind direction, with negative values occurring mostly for SSW winds and positive values for SE. Even if the complexity of the wind plant layout around both sites does not allow for an

https://doi.org/10.5194/wes-2025-198
Preprint. Discussion started: 15 October 2025

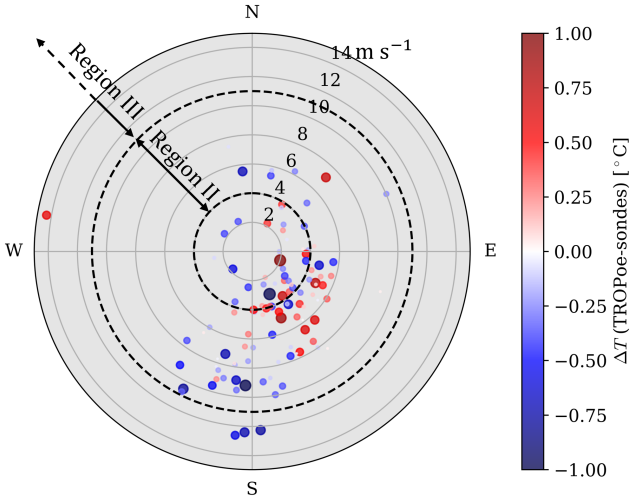

Figure 15. Mean temperature difference TROPoe-sondes below hub height as a function of wind direction and wind speed in the turbine layer. The regions of the turbine power curve are also marked.

easy estimate of wake effects, the directionality of the temperature difference is a strong indication that site-specific conditions (wakes or terrain), rather than instrumental or TROPoe errors, are causing the bias.

We can summarize the main results of this section as follows:

1. Temperature profiles are negligibly biased compared to radiosondes, and the random uncertainty is predicted fairly well by TROPoe.

2. Persistent temperature differences compatible with terrain or wake effects in the lowest 200 m contributed to increasing the RMS of temperature differences close to ground.

4.3 Ability to capture spatial gradients: comparison with surface met sensors

At AWAKEN, each ASSIST was co-located with a surface met station, which offers a unique opportunity to quantify the ability of temperature profiles to capture spatial gradients of temperature near the ground. For this comparison, we use temperature data collected by HMP45C Vaisala platinum resistance temperature detectors installed at 2 m above the ground level. The sensors have an average 1σ uncertainty of 0.25°C (Campbell Scientific, 2007) and are shielded but not actively ventilated. We did not apply any correction for the radiative bias due to the absence of a reliable reference sensor.

The met data are provided natively as a 1-minute average, which is a slower response than that of the ASSIST, so what is shown next will include some representativeness error due to the different sampling rates. In the first place, we characterize the difference between the met and TROPoe output interpolated to 2 m at the same site. The comparison is shown in Fig. 16. The agreement is excellent with an R^2 of 1 to double-digit precision. The slope is consistently less than one, similar to what we found in the pre-campaign test (Fig. 7). Diurnal overheating of the met sensors could also have contributed to reducing the

https://doi.org/10.5194/wes-2025-198
Preprint. Discussion started: 15 October 2025

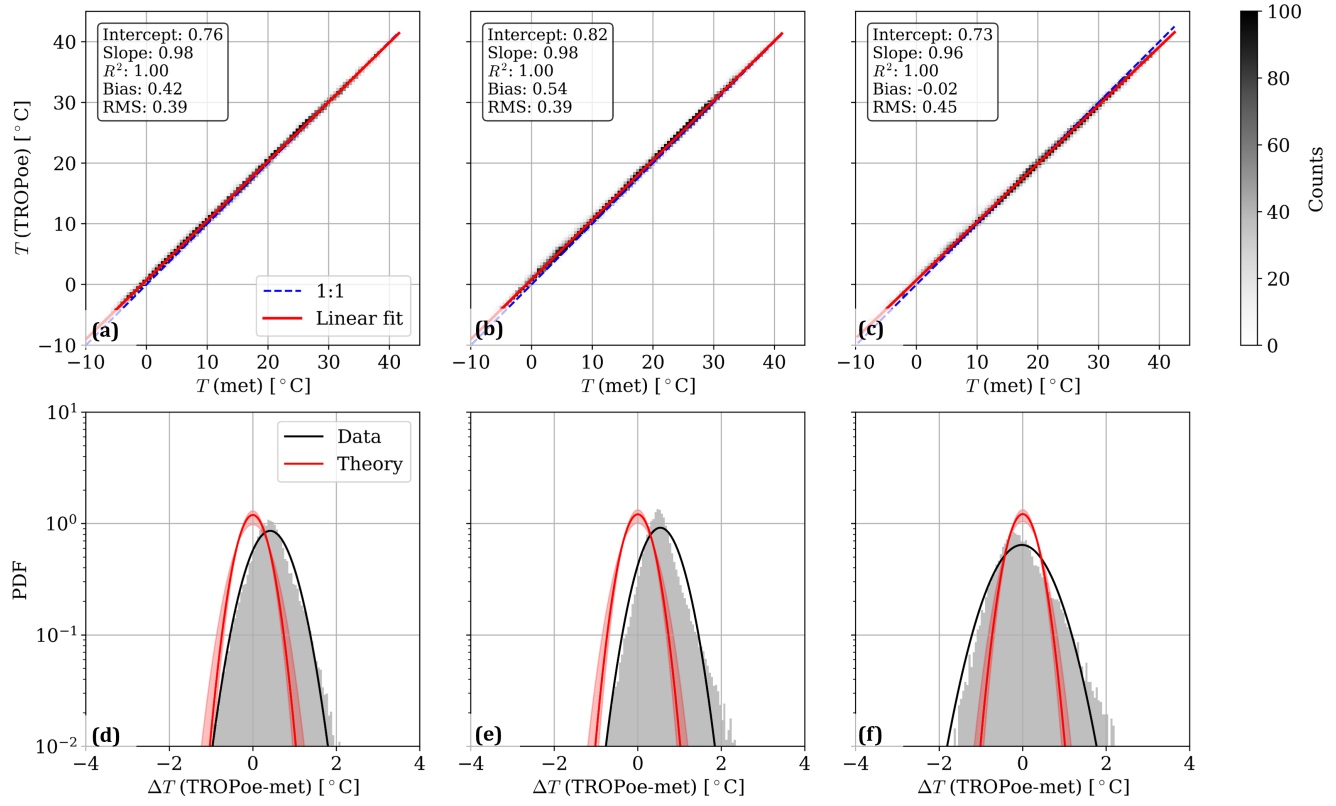

Figure 16. Statistical quantification of the temperature differences between TROPoe and met stations at the same site at 2 m: (a-c) linear regression; (d-f) histograms, where the shaded red area indicates the error PDF using the minimum and maximum combined TROPoe+M5 uncertainty. South site (a,d); Middle site (b,e); North (c,f). site.

slope. Positive biases of about half a degree are seen at the South and Middle sites, while the North site is unbiased. The South ASSIST was the one that showed a much smaller bias with the M5 met tower (Section 3.2). These South and Middle ASSISTs were also the very same used for the side-by-side comparison (Section 3.2), where they showed a negligible bias between each other. Given the pre-campaign results and the fact that the met and ASSIST were co-located at AWAKEN, we speculate that there may be ~ 0.5°C bias in some met sensors. The histograms of temperature differences (Fig. 16, bottom) suggest that the warm bias at the South and Middle sites is pretty consistent, and not due to isolated outliers. It also proves that the uncertainty estimate of TROPoe+met agrees well with the variability seen in the observations (TROPoe uncertainty was, on average, larger at AWAKEN than in the pre-campaign test, mostly due to the different climatologies).

After assessing that TROPoe performs remarkably well in capturing both the surface temperature and its uncertainty at AWAKEN, we move to a more challenging task: quantifying site-to-site temperature gradients. In fact, being a smaller quantity than the absolute temperature, it is more sensitive to inaccuracies. Figure 17 shows the comparison of the temperature

https://doi.org/10.5194/wes-2025-198
Preprint. Discussion started: 15 October 2025

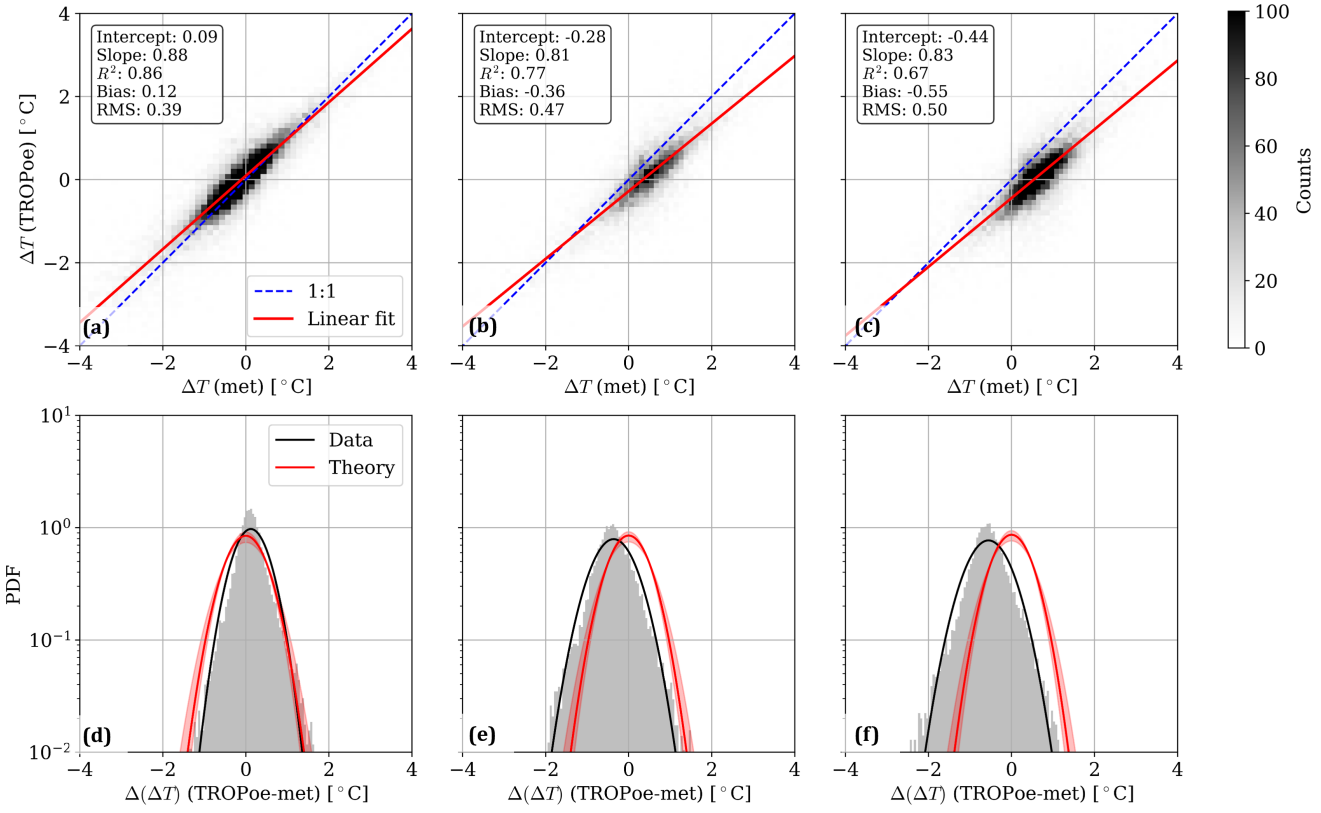

Figure 17. Statistical quantification of the differences between the site-to-site temperature gradients from TROPoe and met stations at 2 m: linear regression (a-c); histograms (d-f), where the shaded red area indicates the error PDF using the minimum and maximum combined TROPoe+M5 uncertainty. Middle - South (a,d); North - South (b,e); North - Middle (c,f).

differences from one site to the other observed through TROPoe and the met. The linear regression shows expectedly poorer metrics than the previous comparison of absolute temperatures, but the agreement remains good. TROPoe can explain between 67% and 86% of the spatial variability of temperature, which is remarkable considering that temperature differences hardly exceed 2°C and detection is done at a relatively high sampling rate (14 s). The agreement of the predicted uncertainty in the site-to-site gradient, $\Delta(\Delta T)$, in Fig. 17d-f, is also satisfactory. The previously observed bias in absolute temperature contributes to shifting the peak of the PDF, but the variability is predicted well by TROPoe+met uncertainty at all sites.

Finally, to check if biases are still dependent on stability as we documented in the pre-campaign test, we calculate the mean temperature difference at the same site, ΔT, and difference in site-to-site gradient, $\Delta(\Delta T)$, for five stability classes. Stability classes are based on the Obukhov length detected by sonics at the nearby sites A2 and A5 (Pekour, 2022a, b) and using the table proposed by Krishnamurthy et al. (2021). As seen from the violin plots in Fig. 18a-c, the differences in absolute temperature do have a mild dependence on stability. The more stable, the warmer the bias in TROPoe vs met, which is consistent with the

https://doi.org/10.5194/wes-2025-198
Preprint. Discussion started: 15 October 2025

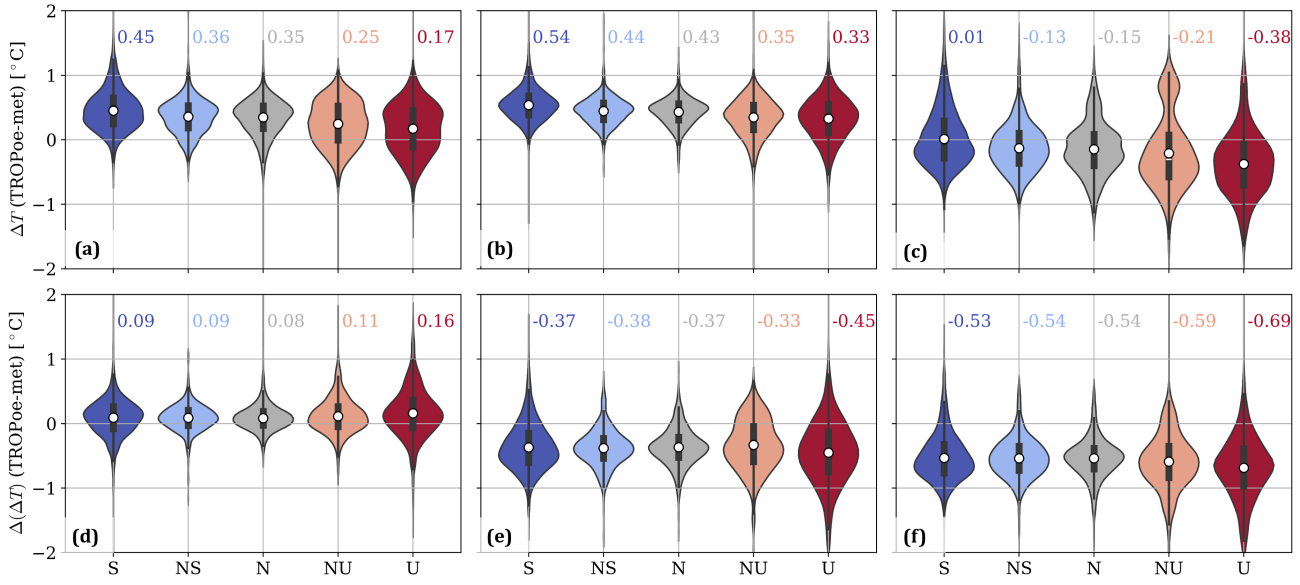

Figure 18. Violin plot of the difference in temperature (a-c) and site-to-site gradient (d-f) between TROPoe and met stations at 2 m for different stabilities: South site (a); Middle site (b); North site (c); Middle - South (d); North - South (e); North - Middle (f). The white dot and the number are the mean value, while the box spans the interquartile range.

pre-campaign results. This dependence is not present when looking at the differences of site-to-site gradients (Fig. 18d-f). This seems to indicate that stability-driven biases in temperature profiles are consistent among different instruments and cancel out when taking the difference.

To conclude the analysis of the AWAKEN dataset and showcase the capabilities of the network of thermodynamic profilers in capturing relevant atmospheric phenomena, we take a close look at an interesting gravity wave event. The wave was likely the result of a bore generated by a thunderstorm located NW of the AWAKEN site, which created gravity waves that traveled across the instrumented domain on August 5th, 2023, from 10:40 to 11:20 UTC (just before sunrise). The event was detected by several permanent weather stations (National Weather Service, 2023; Newsom et al., 2023). The signature of the gravity wave appears most clearly in the reflectivity map of the weather radar in Vance, OK (National Weather Service, 2023). Snapshots of radar reflectivity are shown in Fig. 19, along with corresponding surface temperatures from all AWAKEN met stations (Goldberg, 2023a, b, c, d, e, f, g). We observe an increase in temperature at all sites during the passage of the bore, followed by a drop after 11:18 UTC as the cold air associated with the storm moves in.

The temperature overshoot is poorly understood when relying solely on surface temperature observations. The picture becomes much clearer when we include the temperature profiles (Fig. 20). We can readily identify a stably stratified surface layer before 10:50 UTC that is suddenly disrupted as the bore quickly wipes through. The disruption takes the form of an initial surface warming, whereas the layers of air aloft rapidly cool down. The warming event occurs first at the South and Middle

https://doi.org/10.5194/wes-2025-198
Preprint. Discussion started: 15 October 2025

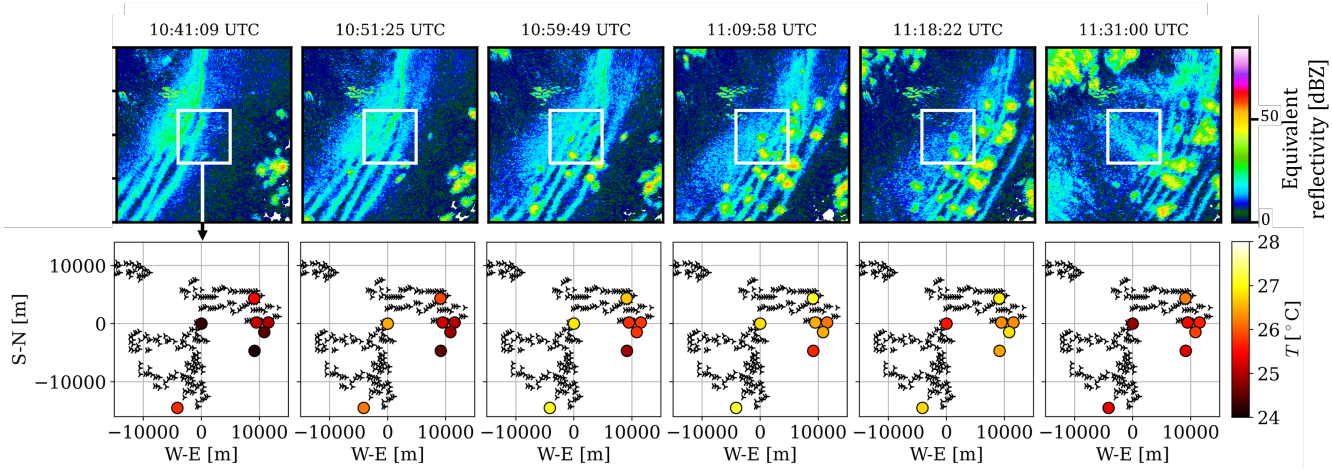

Figure 19. Snapshots of radar reflectivity and corresponding surface temperature from met stations during the wave passage on August 5th, 2023.

site, and then, about 10 minutes later, at the North site, which is consistent with the W-E travel direction of the bore. After 11:20 UTC, the entire boundary layer at all sites eventually experiences the cold air. This is similar to a bore event observed by Haghi et al. (2019) with an AERI system. Another publication based on near-surface observations showed that nocturnal warming events associated with synoptic-scale cold fronts are common in Oklahoma (Nallapareddy et al., 2011). In our case study, we are likely observing a similar phenomenon, but as a result of a thunderstorm outflow.

To summarize, in this section, we learned that:

1. ASSIST+TROPoe temperatures agree extremely well with the measurements from surface stations at AWAKEN, with a nearly perfect R^2 and a bias of < 0.5°C, which is mostly site-dependent and weakly proportional to stability.
2. The TROPoe uncertainty estimate describes well the observed differences with the met stations.
3. The network thermodynamic profilers at AWAKEN is a reliable tool to describe spatial gradients of temperature.

5 Conclusions

We documented the accuracy of temperature profiling methods used at AWAKEN through a four-stage validation exercise. We focused on temperature profiles obtained through the physical retrieval algorithm TROPoe and based on spectral radiance observations of ASSIST passive spectrometers.

First, we compared the difference in temperature profiles between two thermodynamic profilers sitting side-by-side. The bias is negligible and the random error is fairly predicted by TROPoe theory, except very close to the ground, where the tails of the temperature difference distributions are underpredicted.

https://doi.org/10.5194/wes-2025-198
Preprint. Discussion started: 15 October 2025

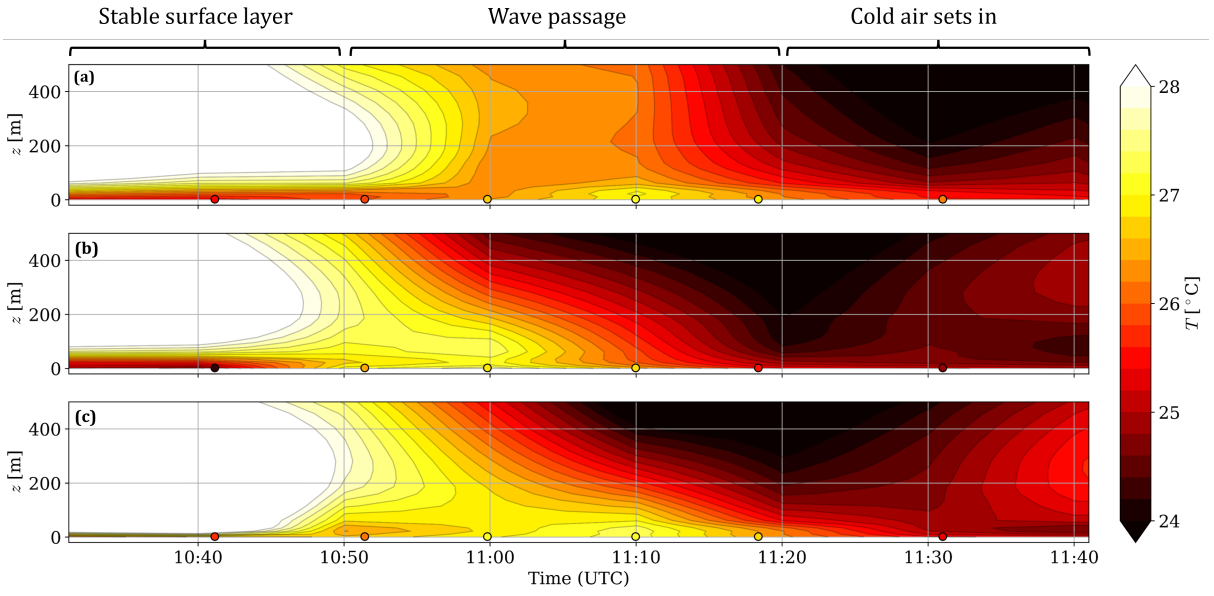

Figure 20. Time-height temperature maps from TROPoe at AWAKEN during a frontal passage on August 5th, 2023: North site (a); Middle site (b); South site (c). The dots are colored according to the temperature from the met station at the respective site.

Second, we assessed the difference between temperature profiles from one thermodynamic profiler and a nearby met mast up to 122 m above the ground. We saw an excellent agreement ($R^2 > 0.98$, negligible bias, and RMS difference of less than 1°C). However, the temperature differences could not be explained solely as the sum of the TROPoe uncertainty estimate, the met sensors' nominal uncertainty, and the spatial decorrelation of thermal turbulence. Indeed, we identified a < 1°C stability-dependent bias whose analysis will be the subject of future work. We also verified the ability of temperature profiles to classify the static stability of the lower ABL, finding 83% and 97% hits for stable and unstable conditions, respectively.

Third, we compared temperature profiles at AWAKEN with 100+ radiosonde observations, reporting a < 0.2°C bias below 2000 m and an RMS that follows the TROPoe prediction quite satisfactorily and never exceeds 1°C below 1000 m.

Finally, we compared the site-to-site temperature gradients at AWAKEN from temperature profiles and surface met station, finding a remarkable accuracy (R^2 between 0.67 and 0.86, bias of 0.5°C and RMS well predicted by TROPoe) even for those small quantities.

In general, we confirmed that the combination of passive infrared spectrometers and physical retrievals allows for a fast, cost-effective, unsupervised, and continuous thermodynamic scanning of the lower atmosphere with traceable uncertainty. These results advocate for a wider use of this temperature profiling technique for wind energy and meteorology applications. Researchers will continue to improve the accuracy of temperature profiling to further reduce or explain the small but detectable differences with met tower observations. Future development efforts will also focus on making temperature profiling

https://doi.org/10.5194/wes-2025-198
Preprint. Discussion started: 15 October 2025

eawe european academy of wind energy
Open Access WIND ENERGY SCIENCE DISCUSSIONS

computationally and logistically less expensive, as well as expanding the data product to gas concentration profiles and cloud properties.

Code availability. The codes used for the data analysis are available at https://github.com/StefanoWind/ASSIST_analysis. The TROPoe processor is available at https://github.com/StefanoWind/TROPoe_processor. TROPoe is available on Docker at https://hub.docker.com/r/davidturner53/tropoe.

Data availability. All data is available on the Wind Data Hub at the URLs provided in the references.

Appendix A: Correction of radiative error in temperature sensors

Lack of aspiration in the temperature sensors is known to cause overheating, especially in high solar radiation and low wind speed conditions (Huwald et al., 2009). During the pre-campaign tests, the temperature sensors on M5 at the heights of 38, 87, and 122 m suffered from a failure in the aspiration system. However, temperature sensors on the M2 tower had operational ventilators for the whole duration of the experiment. Given the homogeneity of thermal conditions at the site, the average temperature difference between M5 and M2 was used as a proxy for the overheating due to solar radiation. This error has been subsequently corrected using the method proposed by Nakamura and Mahrt (2005) and tuned for the present site conditions.

First, the presence of radiative overheating was assessed by calculating mean temperature differences (interpolated) at 38 m as a function of global horizontal irradiance (GHI) and mean horizontal wind speed ($\overline{U}$). The trends of the mean temperature differences, $\Delta\overline{T}$ (M5-M2), can be seen in Fig. A1a. For GHI>0 (daytime), there is a statistically significantly higher temperature at M5, which increases for low wind speed. This is consistent with the presence of radiative overheating at M5. Interestingly, the highest temperature differences occur for moderate rather than high GHI. We speculate that for high GHI, natural convection (not captured in the mean horizontal wind speed) may have contributed to cooling down the sensors. Negative GHI (nighttime) conditions are also showing a slight warming that could not be explained.

As suggested by Nakamura and Mahrt (2005), we estimate the overheating as a function of the scaling parameter:

$$X = \frac{\mathrm{GHI}}{\rho c_p \overline{T}\,\overline{U}}, \tag{A1}$$

where ρ and c_p are the mean density and specific heat capacity of dry air. This quantity represents the ratio of radiative heating by the sun to the convective cooling by the wind. Figure A1b shows the 10-minute and binned mean temperature difference vs. the scaling parameter and the associated linear fit. The slope of the linear fit is fairly close to the one provided in the original paper (434.76 vs. 373.40), hinting at a similar heat transfer physics between the M5 sensors and those of Nakamura and Mahrt (2005). Still, the linear fit could explain only 32% of the variance in the data, which suggests that other effects may have played a role (wind direction, spatial inhomogeneity, etc). The linear correction in Fig. A1b based on 10-minute averaged

https://doi.org/10.5194/wes-2025-198
Preprint. Discussion started: 15 October 2025

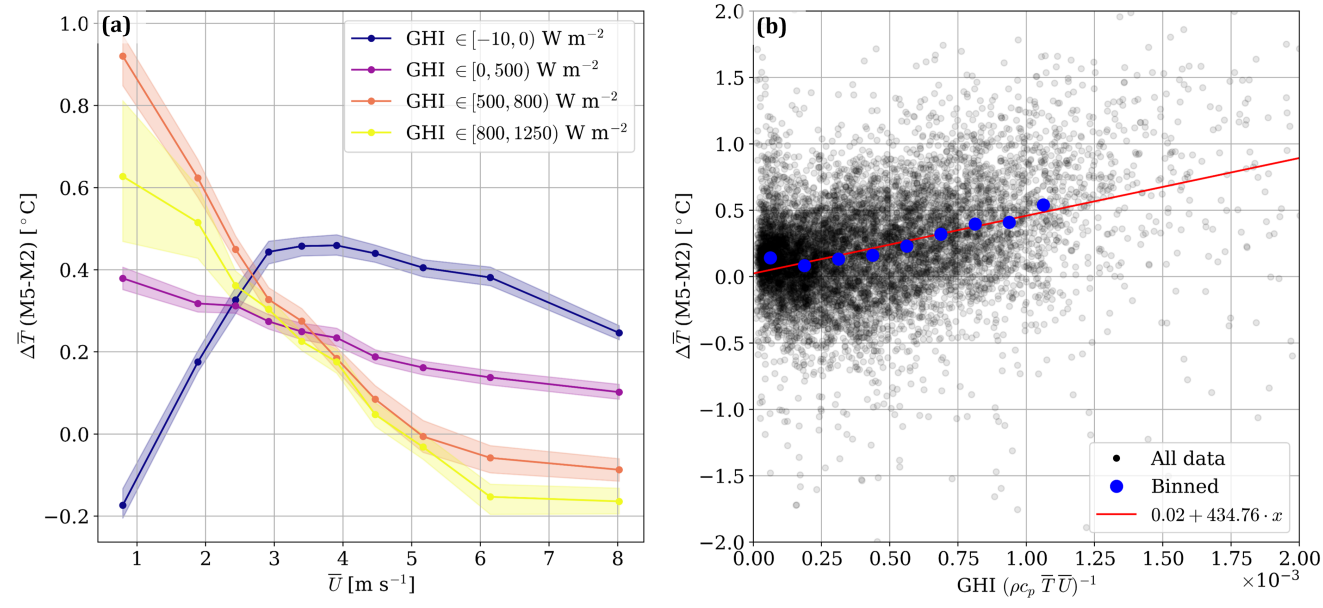

Figure A1. Summary of the aspiration correction: mean temperature difference M5-M2 at 38 m for different global horizontal irradiances and mean horizontal wind speeds, where the shaded area represents the 95% c.i. (a); linear fit of radiative error vs. overheating scaling parameter (b).

temperatures, wind speed, and GHI was applied to all M5 data and contributed to an average ~ 0.2°C drop in peak daytime temperature and a ~ 10 - 15% reduction in RMS of the temperature difference between TROPoe and M5.

Author contributions. SL conceptualized the study, led the analysis, and wrote the original draft. DDT is the primary developer of TROPoe, provided scientific guidance on its analysis, and helped process the data. AA contributed to Section 4.3. PJM handled funding for the AWAKEN project. LR provided logistical support. All authors reviewed the manuscript.

Competing interests. The contact author has declared that none of the authors has any competing interests.

Disclaimer. This work was authored in part by the National Renewable Energy Laboratory (NREL) for the U.S. Department of Energy (DOE) under Contract No. DE-AC36-08GO28308. Funding was provided by the U.S. Department of Energy Office of Energy Efficiency and Renewable Energy Wind Energy Technologies Office and the National Oceanic and Atmospheric Administration (NOAA) Atmospheric Science for Renewable Energy Program. The views expressed in the article do not necessarily represent the views of the DOE, NOAA, or

https://doi.org/10.5194/wes-2025-198
Preprint. Discussion started: 15 October 2025

545 the U.S. Government. The publisher, by accepting the article for publication, acknowledges that the U.S. Government retains a nonexclusive, paid-up, irrevocable, worldwide license to publish or reproduce the published form of this work, or allow others to do so, for U.S. Government purposes.

Acknowledgements. Thanks to Adam Wise and Brian Hirth for their insightful comments on the bore event discussed in Section 4.3 and to Yelena Pichugina for providing lidar data that helped finalize Section 3.1.

https://doi.org/10.5194/wes-2025-198
Preprint. Discussion started: 15 October 2025

eawe european academy of wind energy
Open Access WIND ENERGY SCIENCE DISCUSSIONS

References

Abkar, M. and Porté-Agel, F.: Influence of atmospheric stability on wind-turbine wakes: A large-eddy simulation study, Physics of Fluids, 27, https://doi.org/10.1063/1.4913695, 2015.

Abraham, A., Puccioni, M., Jordan, A., Maric, E., Bodini, N., Hamilton, N., Letizia, S., Klein, P. M., Smith, E. N., Wharton, S., Gero, J., Jacob, J. D., Krishnamurthy, R., Newsom, R. K., Pekour, M., Radünz, W., and Moriarty, P.: Operational wind plants increase planetary boundary layer height: an observational study, Wind Energy Science, 10, 1681–1705, https://doi.org/10.5194/wes-10-1681-2025, 2025.

Adler, B., Turner, D. D., Bianco, L., Djalalova, I. V., Myers, T., and Wilczak, J. M.: Improving solution availability and temporal consistency of an optimal estimation physical retrieval for ground-based thermodynamic boundary layer profiling, Atmospheric Measurement Techniques, 17, 6603–6624, https://doi.org/10.5194/egusphere-2024-714, 2024.

Aitken, M. L., Banta, R. M., Pichugina, Y. L., and Lundquist, J. K.: Quantifying Wind Turbine Wake Characteristics from Scanning Remote Sensor Data, Journal of Atmospheric and Oceanic Technology, 31, 765–787, https://doi.org/10.1175/JTECH-D-13-00104.1, 2014.

Baidya Roy, S. and Traiteur, J. J.: Impacts of wind farms on surface air temperatures, Proceedings of the National Academy of Sciences, 107, 17 899–17 904, https://doi.org/10.1073/pnas.1000493107, 2010.

Bianco, L., Adler, B., Bariteau, L., Djalalova, I. V., Myers, T., Pezoa, S., Turner, D. D., and Wilczak, J. M.: Sensitivity of thermodynamic profiles retrieved from ground-based microwave and infrared observations to additional input data from active remote sensing instruments and numerical weather prediction models, Atmospheric Measurement Techniques, 17, 3933–3948, https://doi.org/10.5194/amt-17-3933-2024, 2024.

Blumberg, W. G., Turner, D. D., Löhnert, U., and Castleberry, S.: Ground-based temperature and humidity profiling using spectral infrared and microwave observations. Part II: Actual retrieval performance in clear-sky and cloudy conditions, Journal of Applied Meteorology and Climatology, 54, 2305–2319, https://doi.org/10.1175/JAMC-D-15-0005.1, 2015.

Blumberg, W. G., Wagner, T. J., Turner, D. D., and Correia, J.: Quantifying the accuracy and uncertainty of diurnal thermodynamic profiles and convection indices derived from the atmospheric emitted radiance interferometer, Journal of Applied Meteorology and Climatology, 56, 2747–2766, https://doi.org/10.1175/JAMC-D-17-0036.1, 2017.

Bodini, N., Optis, M., Liu, Y., Gaudet, B., Krishnamurthy, R., Kumler, A., Rosencrans, D., Rybchuk, A., Tai, S.-L., Berg, L., Musial, W., Lundquist, J. K., Purkayastha, A., Young, E., and Draxl, C.: Causes of and Solutions to Wind Speed Bias in NREL's 2020 Offshore Wind Resource Assessment for the California Pacific Outer Continental Shelf Renewable and Sustainable Energy Institute, Tech. Rep. February 2024, National Renewable Energy Laboratory, Golden, CO, www.nrel.gov/publications., 2024.

Campbell Scientific: Model HMP45C Temperature and Relative Humidity Probe Instruction Manual, Campbell Scientific, https://s.campbellsci.com/documents/af/manuals/hmp45c.pdf, available as PDF from Campbell Scientific website, 2007.

Chamorro, L. P. and Porté-Agel, F.: Effects of Thermal Stability and Incoming Boundary-Layer Flow Characteristics on Wind-Turbine Wakes: A Wind-Tunnel Study, Boundary-Layer Meteorology, 136, 515–533, https://doi.org/10.1007/s10546-010-9512-1, 2010.

Clifton, A.: 135-m Meteorological Masts at the National Wind Technology Center, Tech. Rep. July, National Renewable Energy Laboratory, Golden, CO, 2014.

Clough, S. A., Shephard, M. W., Mlawer, E. J., Delamere, J. S., Iacono, M. J., Cady-Pereira, K., Boukabara, S., and Brown, P. D.: Atmospheric radiative transfer modeling: A summary of the AER codes, Journal of Quantitative Spectroscopy and Radiative Transfer, 91, 233–244, https://doi.org/10.1016/j.jqsrt.2004.05.058, 2005.

https://doi.org/10.5194/wes-2025-198
Preprint. Discussion started: 15 October 2025

de Silva, C. M., Marusic, I., Woodcock, J. D., and Meneveau, C.: Scaling of second- and higher-order structure functions in turbulent boundary layers, Journal of Fluid Mechanics, 769, 654–686, 2015.

Doubrawa, P., Quon, E. W., Martinez-Tossas, L. A., Shaler, K., Debnath, M., Hamilton, N., Herges, T. G., Maniaci, D., Kelley, C. L., Hsieh, A. S., Blaylock, M. L., van der Laan, P., Andersen, S. J., Krueger, S., Cathelain, M., Schlez, W., Jonkman, J., Branlard, E., Steinfeld, G., Schmidt, S., Blondel, F., Lukassen, L. J., and Moriarty, P.: Multimodel validation of single wakes in neutral and stratified atmospheric conditions, Wind Energy, pp. 1–29, https://doi.org/10.1002/we.2543, 2020.

Frost, C. and Thompson, S. G.: Correcting for regression dilution bias: comparison of methods for a single predictor variable, Journal of the Royal Statistical Society: Series A (Statistics in Society), 163, 173–189, https://doi.org/10.1111/1467-985X.00164, 2000.

Goldberg, L.: Site A1 - Surface Meteorological Station / Reviewed Data, https://doi.org/10.21947/1959687, accessed: 2025-08-26, 2023a.

Goldberg, L.: Site A2 - Surface Meteorological Station / Reviewed Data, https://doi.org/10.21947/1959689, accessed: 2025-08-26, 2023b.

Goldberg, L.: Site A5 - Surface Meteorological Station / Reviewed Data, https://doi.org/10.21947/1959693, accessed: 2025-08-26, 2023c.

Goldberg, L.: Site A7 - Surface Meteorological Station / Reviewed Data, https://doi.org/10.21947/1959695, accessed: 2025-08-26, 2023d.

Goldberg, L.: Site B - Surface Meteorological Station / Reviewed Data, https://doi.org/10.21947/2570093, accessed: 2025-08-26, 2023e.

Goldberg, L.: Site C1a - Surface Meteorological Station / Reviewed Data, https://doi.org/10.21947/1959700, accessed: 2025-08-26, 2023f.

Goldberg, L.: Site G - Surface Meteorological Station / Reviewed Data, https://doi.org/10.21947/1959708, accessed: 2025-08-26, 2023g.

Haghi, K. R., Geerts, B., Chipilski, H. G., Johnson, A., Degelia, S., Imy, D., Parsons, D. B., Adams-Selin, R. D., Turner, D. D., and Wang, X.: Bore-ing into Nocturnal Convection, Bulletin of the American Meteorological Society, 100, 1103–1121, https://doi.org/10.1175/BAMS-D-17-0250.1, 2019.

Hamilton, N.: NWTC Ceilometer (1) Pre-campaign / Reviewed Data, https://wdh.energy.gov/ds/awaken/nwtc.ceil.z01.b0, accessed: 2025-08-26, 2022.

Hamilton, N.: AWAKEN Site A1 - NREL Ceilometer (Vaisala CL51) / Reviewed Data, https://doi.org/10.21947/2221790, accessed: 2025-08-26, 2023.

Hamilton, N. and Debnath, M.: National Wind Technology Center-Characterization of Atmospheric Conditions, Tech. Rep. August, National Renewable Energy Laboratory, 2019.

Han, G. and Zhang, X.: Applicability of Taylor's frozen hypothesis and elliptic model in the atmospheric surface layer, Boundary-Layer Meteorology, 184, 423–440, https://doi.org/10.1007/s10546-022-00711-y, 2022.

Holdridge, D.: Balloon-Borne Sounding System (SONDE) Instrument Handbook, Tech. rep., Atmospheric Radiation Measurement, https://www.arm.gov/publications/tech_reports/handbooks/sonde_handbook.pdf, 2020.

Huwald, H., Higgins, C. W., Boldi, M.-O., Bou-Zeid, E. R., Lehning, M., and Parlange, M. B.: Albedo effect on radiative errors in air temperature measurements, Water Resources Research, 45, W08 431, https://doi.org/10.1029/2008WR007600, 2009.

International Electrotechnical Commission: IEC 61400-12-1:2022 - Wind energy generation systems – Part 12-1: Power performance measurements of electricity producing wind turbines, https://webstore.iec.ch/publication/69093, iEC Standard, 2022.

International Energy Agency: Electricity 2025: Analysis and forecast to 2027, Tech. rep., International Energy Agency, https://iea.blob.core.windows.net/assets/0f028d5f-26b1-47ca-ad2a-5ca3103d070a/Electricity2025.pdf, cC BY 4.0, 2025.

Keeler, E., Burk, K., and Kyrouac, J.: Balloon-Borne Sounding System (SONDEWNPN), 2023-04-10 to 2023-08-22, Southern Great Plains (SGP), Billings, OK (Site H for AWAKEN) (S6), https://doi.org/10.5439/1595321, 2023.

https://doi.org/10.5194/wes-2025-198
Preprint. Discussion started: 15 October 2025

Keith, D. W., DeCarolis, J. F., Denkenberger, D. C., Lenschow, D. H., Malyshev, S. L., Pacala, S., and Rasch, P. J.: The Influence of Large-Scale Wind Power on Global Climate, Proceedings of the National Academy of Sciences, 101, 16 115–16 120, https://doi.org/10.1073/pnas.0406930101, 2004.

Klein, P., Bonin, T. A., Newman, J. F., Turner, D. D., Chilson, P. B., Wainwright, C. E., Blumberg, W. G., Mishra, S., Carney, M., Jacacobsen, E. P., Wharton, S., and Newsom, R. K.: LABLE: A multi-institutional, student-led, atmospheric boundary layer experiment, Bulletin of the American Meteorological Society, 96, 1743–1764, https://doi.org/10.1175/BAMS-D-13-00267.1, 2015.

Knuteson, R. O., Revercomb, H. E., Best, F. A., Ciganovich, N. C., Dedecker, R. G., Dirkx, T. P., Ellington, S. C., Feltz, W. F., Garcia, R. K., Howell, H. B., Smith, W. L., Short, J. F., and Tobin, D. C.: Atmospheric Emitted Radiance Interferometer. Part I: Instrument design, Journal of Atmospheric and Oceanic Technology, 21, 1763–1776, https://doi.org/10.1175/JTECH-1662.1, 2004a.

Knuteson, R. O., Revercomb, H. E., Best, F. A., Ciganovich, N. C., Dedecker, R. G., Dirkx, T. P., Ellington, S. C., Feltz, W. F., Garcia, R. K., Howell, H. B., Smith, W. L., Short, J. F., and Tobin, D. C.: Atmospheric Emitted Radiance Interferometer. Part II: Instrument performance, Journal of Atmospheric and Oceanic Technology, 21, 1777–1789, https://doi.org/10.1175/JTECH-1663.1, 2004b.

Krishnamurthy, R., Newsom, R. K., Chand, D., and Shaw, W. J.: Boundary Layer Climatology at ARM Southern Great Plains, Tech. Rep. PNNL-30832, Pacific Northwest National Laboratory (PNNL), https://www.pnnl.gov/main/publications/external/technical_reports/PNNL-30832.pdf, accessed: 2025-08-20, 2021.

Krishnamurthy, R., Newsom, R. K., Kaul, C. M., Letizia, S., Pekour, M., Hamilton, N., Chand, D., Flynn, D., Bodini, N., and Moriarty, P.: Observations of Wind Farm Wake Recovery at an Operating Wind Farm, Wind Energy Science, 10, 361–380, https://doi.org/10.5194/wes-10-361-2025, 2025.

Lee, J. C. Y. and Fields, M. J.: An overview of wind-energy-production prediction bias, losses, and uncertainties, Wind Energy Science, 6, 311–365, https://doi.org/10.5194/wes-6-311-2021, 2021.

Letizia, S.: NWTC Thermodynamic Profiler (Assist II-10) Pre-campaign / Summary Data, https://wdh.energy.gov/ds/awaken/nwtc.assist.z01.00, accessed: 2025-08-26, 2022a.

Letizia, S.: NWTC Thermodynamic Profiler (Assist II-11) Pre-campaign / Summary Data, https://wdh.energy.gov/ds/awaken/nwtc.assist.z02.00, accessed: 2025-08-26, 2022b.

Letizia, S.: NWTC Thermodynamic Profiler (Assist II-12) Pre-campaign / Summary Data, https://wdh.energy.gov/ds/awaken/nwtc.assist.z03.00, accessed: 2025-08-26, 2022c.

Letizia, S., Robey, R., Bodini, N., Krishnamurthy, R., Moriarty, P. J., Gomez, M. S., Lundquist, J. K., Robey, R., and Gomez, M. S.: Tilted lidar profiling: Development and testing of a novel scanning strategy for inhomogeneous flows, Journal of Renewable and Sustainable Energy, 16, https://doi.org/10.1063/5.0209729, 2024.

Letizia, S., Michaud-Belleau, V., Turner, D. D., and Abraham, A.: Thermodynamic Profiling Through ASSIST Observations and TROPoe Retrievals, Technical Report NREL/XXXX-XXXXX, National Renewable Energy Laboratory (NREL), Golden, CO, 2025.

Li, Y., Kalnay, E., Motesharrei, S., Rivas, J., Kucharski, F., Kirk-Davidoff, D., Bach, E., and Zeng, N.: Climate model shows large-scale wind and solar farms in the Sahara increase rain and vegetation, Science, 361, 1019–1022, https://doi.org/10.1126/science.aar5629, 2018.

Liu, N., Zhao, X., Zhang, X., Zhao, J., Wang, H., and Wu, D.: Remotely Sensed Evidence of the Divergent Climate Impacts of Wind Farms on Croplands and Grasslands, Science of the Total Environment, 905, 167 203, https://doi.org/10.1016/j.scitotenv.2023.167203, 2023.

Maahn, M., Turner, D. D., Löhnert, U., Posselt, D. J., Ebell, K., Mace, G. G., and Comstock, J. M.: Optimal estimation retrievals and their uncertainties, Bulletin of the American Meteorological Society, 101, E1512–E1523, https://doi.org/10.1175/BAMS-D-19-0027.1, 2020.

https://doi.org/10.5194/wes-2025-198
Preprint. Discussion started: 15 October 2025

Mahrt, L., Belušić, D., and Acevedo, O.: Small-Scale Spatial Variation of the Nocturnal Wind Field, Boundary-Layer Meteorology, 180, 225–245, https://doi.org/10.1007/s10546-021-00627-z, 2021.

Michaud-Belleau, V., Gaudreau, M., Lacoursière, J., Boisvert, E., Ravelomanantsoa, L., Turner, D. D., and Rochette, L.: The Atmospheric Sounder Spectrometer by Infrared Spectral Technology (ASSIST): instrument design and signal processing, Atmospheric Measurement Techniques, 18, 3585–3609, https://doi.org/10.5194/amt-18-3585-2025, 2025.

Miller, L. M. and Keith, D. W.: Climatic Impacts of Wind Power, Joule, 2, 2618–2632, https://doi.org/10.1016/j.joule.2018.09.009, 2018.

Mlawer, E. J. and Turner, D. D.: Spectral Radiation Measurements and Analysis in the ARM Program, Meteorological Monographs, 57, 14.1–14.17, https://doi.org/10.1175/amsmonographs-d-15-0027.1, 2016.

Moravec, D., Barták, V., and Puš, V.: Wind turbine impact on near-ground air temperature, Renewable Energy, 123, 627–633, https://doi.org/10.1016/j.renene.2018.02.049, 2018.

Moriarty, P., Bodini, N., Letizia, S., Abraham, A., Ashley, T., Bärfuss, K. B., Barthelmie, R. J., Brewer, A., Brugger, P., Feuerle, T., et al.: Overview of preparation for the American Wake Experiment (AWAKEN), Journal of Renewable and Sustainable Energy, 16, 2024.

Nakamura, R. and Mahrt, L.: Air Temperature Measurement Errors in Naturally Ventilated Radiation Shields, Journal of Atmospheric and Oceanic Technology, 22, 1046–1058, https://doi.org/10.1175/JTECH1762.1, 2005.

Nallapareddy, A., Shapiro, A., and Gourley, J. J.: A Climatology of Nocturnal Warming Events Associated with Cold-Frontal Passages in Oklahoma, Journal of Applied Meteorology and Climatology, 50, 2042–2061, https://doi.org/10.1175/JAMC-D-11-020.1, 2011.

National Weather Service: WSR-88D Radar (Weather Surveillance Radar-1988 Doppler), https://www.weather.gov/iwx/wsr_88d, accessed: 2025-08-26, 2023.

Newsom, R., Shi, Y., and Krishnamurthy, R.: Doppler Lidar (DLFPT), 2010-10-22 to 2025-08-04, Southern Great Plains (SGP), Central Facility, Lamont, OK (C1), https://doi.org/10.5439/1025185, 2023.

Pekour, M.: Site A2 - PNNL Surface Flux Station / Daily Fluxes, https://doi.org/10.21947/1899850, accessed: 2025-08-26, 2022a.

Pekour, M.: Site A5 - PNNL Surface Flux Station / Daily Fluxes, https://doi.org/10.21947/1899848, accessed: 2025-08-26, 2022b.

Radünz, W., Souza Carmo, B., Lundquist, J. K., Letizia, S., Abraham, A., Wise, A. S., Sanchez Gomez, M., Hamilton, N., Rai, R. K., and Peixoto, P. S.: Influence of simple terrain on the spatial variability of a low-level jet and wind farm performance in the AWAKEN field campaign, Wind Energy Science Discussions, 2024.

Rajewski, D. A., Takle, E. S., Lundquist, J. K., Oncley, S., Prueger, J. H., Horst, T. W., Rhodes, M. E., Pfeiffer, R., Hatfield, J. L., Spoth, K. K., and Doorenbos, R. K.: Crop Wind Energy Experiment (CWEX): Observations of Surface-Layer, Boundary Layer, and Mesoscale Interactions with a Wind Farm, Bulletin of the American Meteorological Society, 94, 655–672, https://doi.org/10.1175/BAMS-D-11-00240.1, 2013.

Rodgers, C. D.: Inverse methods for atmospheric sounding: theory and practice, vol. 2, World scientific, 2000.

Shaw, W. J., Berg, L. K., Debnath, M., Deskos, G., Draxl, C., Ghate, V. P., Hasager, C. B., Kotamarthi, R., Mirocha, J. D., Muradyan, P., Pringle, W. J., Turner, D. D., and Wilczak, J. M.: Scientific challenges to characterizing the wind resource in the marine atmospheric boundary layer, Wind Energy Science, 7, 2307–2334, https://doi.org/10.5194/wes-7-2307-2022, 2022.

Shippert, T., Newsom, R., Riihimaki, L., and Zhang, D.: Doppler Lidar Vertical Velocity Statistics (DLPROFWSTATS4NEWS), 2016-05-03 to 2023-11-01, Southern Great Plains (SGP), Waukomis, OK (Extended) (E37), https://doi.org/10.5439/1178583, 2023.

Siegel, R.: Thermal Radiation Heat Transfer: Vol. 3: Radiation Transfer with Absorbing, Emitting, and Scattering Media, vol. 164, Scientific and Technical Information Division, National Aeronautics and Space Administration, 1971.

https://doi.org/10.5194/wes-2025-198
Preprint. Discussion started: 15 October 2025

Smith, C. M., Barthelmie, R. J., and Pryor, S. C.: In situ observations of the influence of a large onshore wind farm on near-surface temperature, turbulence intensity and wind speed profiles, Environmental Research Letters, 8, 034 006, https://doi.org/10.1088/1748-9326/8/3/034006, 2013.

St.Martin, C. M., Lundquist, J. K., Clifton, A., Poulos, G. S., and Schreck, S. J.: Wind turbine power production and annual energy production depend on atmospheric stability and turbulence, Wind Energy Science, 1, 221–236, https://doi.org/10.5194/wes-1-221-2016, 2016.

Stull, R. B.: An Introduction to Boundary Layer Meteorology, Springer, Dordrecht, ISBN 978-90-277-2768-8, https://doi.org/10.1007/978-94-009-3027-8, 1988.

Sun, J., Mahrt, L., Nappo, C., and Lenschow, D. H.: Wind and Temperature Oscillations Generated by Wave–Turbulence Interactions in the Stably Stratified Boundary Layer, Journal of the Atmospheric Sciences, 72, 1484–1503, https://doi.org/10.1175/JAS-D-14-0129.1, 2015.

Taylor, G. I.: The Spectrum of Turbulence, Proceedings of the Royal Society of London. Series A, Mathematical and Physical Sciences, 164, 476–490, https://doi.org/10.1098/rspa.1938.0032, 1938.

Turner, D.: TROPOe Docker Image, https://hub.docker.com/r/davidturner53/tropoe, accessed: 2025-04-25, 2025.

Turner, D., Adler, B., Bianco, L., Wilczak, J., Michaud-Belleau, V., and Rochette, L.: Intercomparison of seven collocated ground-based interferrometers and retrieved thermodynamic profiles, Submitted to Atmospheric Measurement Techniques, 2025.

Turner, D. D. and Blumberg, W. G.: Improvements to the AERIoe thermodynamic profile retrieval algorithm, IEEE Journal of Selected Topics in Applied Earth Observations and Remote Sensing, 12, 1339–1354, https://doi.org/10.1109/JSTARS.2018.2874968, 2019.

Turner, D. D. and Löhnert, U.: Information content and uncertainties in thermodynamic profiles and liquid cloud properties retrieved from the ground-based Atmospheric Emitted Radiance Interferometer (AERI), Journal of Applied Meteorology and Climatology, 53, 752–771, https://doi.org/10.1175/JAMC-D-13-0126.1, 2014.

Turner, D. D. and Löhnert, U.: Ground-based temperature and humidity profiling: Combining active and passive remote sensors, Atmospheric Measurement Techniques, 14, 3033–3048, https://doi.org/10.5194/amt-14-3033-2021, 2021.

Turner, D. D., Tobin, D. C., Clough, S. A., Brown, P. D., Ellingson, R. G., Mlawer, E. J., Knuteson, R. O., Revercomb, H. E., Shippert, T. R., Smith, W. L., and Shephard, M. W.: The QME AERI LBLRTM: A closure experiment for downwelling high spectral resolution infrared radiance, Journal of the Atmospheric Sciences, 61, 2657–2675, https://doi.org/10.1175/JAS3300.1, 2004.

Turner, D. D., Knuteson, R. O., Revercomb, H. E., Lo, C., and Dedecker, R. G.: Noise Reduction of Atmospheric Emitted Radiance Interferometer (AERI) Observations Using Principal Component Analysis, Journal of Atmospheric and Oceanic Technology, 23, 1223–1238, https://doi.org/10.1175/JTECH1906.1, 2006.

Veers, P., Dykes, K., Lantz, E., Barth, S., Bottasso, C. L., Carlson, O., Clifton, A., Green, J., Green, P., Holttinen, H., Laird, D., Lehtomäki, V., Lundquist, J. K., Manwell, J., Marquis, M., Meneveau, C., Moriarty, P., Munduate, X., Muskulus, M., Naughton, J., Pao, L., Paquette, J., Peinke, J., Robertson, A., Sanz Rodrigo, J., Sempreviva, A. M., Smith, J. C., Tuohy, A., and Wiser, R.: Grand challenges in the science of wind energy, Science, 366, eaau2027, https://doi.org/10.1126/science.aau2027, 2019.

Walsh-Thomas, J. M., Cervone, G., Agouris, P., and Manca, G.: Further evidence of impacts of large-scale wind farms on land surface temperature, Renewable and Sustainable Energy Reviews, 16, 6432–6437, https://doi.org/10.1016/j.rser.2012.07.004, 2012.

Wang, C. and Prinn, R. G.: Potential Climatic Impacts and Reliability of Very Large-Scale Wind Farms, Atmospheric Chemistry and Physics, 10, 2053–2061, https://doi.org/10.5194/acp-10-2053-2010, 2010.

Wang, H., Barthelmie, R. J., Clifton, A., and Pryor, S. C.: Wind measurements from arc scans with Doppler wind lidar, Journal of Atmospheric and Oceanic Technology, 32, 2024–2040, https://doi.org/10.1175/JTECH-D-14-00059.1, 2015.

https://doi.org/10.5194/wes-2025-198
Preprint. Discussion started: 15 October 2025

Wu, S. and Archer, C. L.: Near-Ground Effects of Wind Turbines: Observations and Physical Mechanisms, Monthly Weather Review, 149, 879–898, https://doi.org/10.1175/MWR-D-20-0186.1, 2021.

Wu, S., Archer, C. L., and Mirocha, J. D.: New Insights on Wind Turbine Wakes from Large-Eddy Simulation: Wake Contraction, Dual Nature, and Temperature Effects, Wind Energy, 27, https://doi.org/10.1002/we.2827, 2023.

Wyngaard, J.: On Surface Layer Turbulence, pp. 101–149, American Meteorological Society, Boston, 1973.

Wyngaard, J., Izumi, Y., and Collins, S.: Behavior of the Refractive-Index-Structure Parameter near the Ground, Journal of the Optical Society of America, 61, 1646–1650, https://doi.org/10.1364/JOSA.61.001646, 1971.

Xia, G., Zhou, L., Freedman, J. M., Baidya Roy, S., Harris, R. A., and Cervarich, M. C.: A case study of effects of atmospheric boundary layer turbulence, wind speed, and stability on wind farm induced temperature changes using observations from a field campaign, Climate Dynamics, 46, 2179–2196, https://doi.org/10.1007/s00382-015-2696-9, 2016.

Xia, G., Zhou, L., Minder, J. R., Fovell, R. G., and Jiménez, P. A.: Simulating Impacts of Real-World Wind Farms on Land Surface Temperature Using the WRF Model: Physical Mechanisms, Climate Dynamics, 53, 1723–1739, https://doi.org/10.1007/s00382-019-04725-0, 2019.

Zhan, L., Letizia, S., and Iungo, G. V.: LiDAR measurements for an onshore wind farm : Wake variability for different incoming wind speeds and atmospheric stability regimes, Wind Energy, pp. 1–27, https://doi.org/10.1002/we.2430, 2019.

Zhang, D., Ermold, B., and Morris, V.: Ceilometer (CEIL), 1997-09-14 to 2025-08-25, Southern Great Plains (SGP), Central Facility, Lamont, OK (C1), https://doi.org/10.5439/1181954, 2023a.

Zhang, D., Ermold, B., and Morris, V.: Ceilometer (CEIL), 2022-11-29 to 2023-09-07, Southern Great Plains (SGP), Billings, OK (Site H for AWAKEN) (S6), https://doi.org/10.5439/1181954, 2023b.

Zhou, L., Tian, Y., Baidya Roy, S., Thorncroft, C., Bosart, L. F., and Hu, Y.: Impacts of wind farms on land surface temperature, Nature Climate Change, 2, 539–543, https://doi.org/10.1038/nclimate1505, 2012.

Zhou, L., Tian, Y., Baidya Roy, S., Dai, Y., and Chen, H.: Diurnal and seasonal variations of wind farm impacts on land surface temperature over western Texas, Climate Dynamics, 41, 307–326, https://doi.org/10.1007/s00382-012-1485-y, 2013.